

**MICROELECTROMECHANICAL SCANNER USING
A VERTICAL CAVITY SURFACE EMITTING LASER**

THESIS

Joseph G. Bouchard Jr., Captain, USAF

AFIT/GCS/ENG/97D-04

DTIC QUALITY INSPECTED 4

DISTRIBUTION STATEMENT A

**Approved for public release
Distribution Unlimited**

**DEPARTMENT OF THE AIR FORCE
AIR UNIVERSITY**

AIR FORCE INSTITUTE OF TECHNOLOGY

Wright-Patterson Air Force Base, Ohio

19980210 055

AFIT/GCS/ENG/97D-04

**MICROELECTROMECHANICAL SCANNER USING
A VERTICAL CAVITY SURFACE EMITTING LASER**

THESIS

Joseph G. Bouchard Jr., Captain, USAF

AFIT/GCS/ENG/97D-04

Approved for public release; distribution unlimited

The views expressed in this thesis are those of the author and do not reflect the official policy or position of the Department of Defense of the U. S. Government

AFIT/GCS/ENG/97D-04

**MICROELECTROMECHANICAL SCANNER USING
A VERTICAL CAVITY SURFACE EMITTING LASER**

THESIS

**Presented to the Faculty of the Graduate School of Engineering
of the Air Force Institute of Technology
Air University
Air Education and Training Command
in Partial Fulfillment of the
Requirements for the Degree of
Master of Science in Computer Engineering**

**Joseph G. Bouchard Jr., B.S.
Captain, USAF**

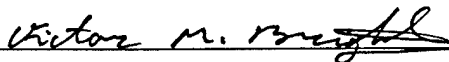
December 1997

Approved for public release; distribution unlimited

**MICROELECTROMECHANICAL SCANNER USING
A VERTICAL CAVITY SURFACE EMITTING LASER**

**Joseph G. Bouchard Jr., BS EE
Captain, USAF**

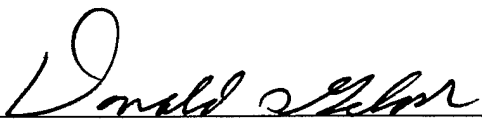
Approved:



Dr. Victor M. Bright , Chairman

24 Nov. '97

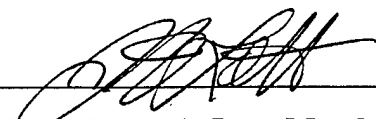
date



Major Donald S. Gelosh, Member

24 Nov 97

date



Major James A. Lott, Member

24 NOV 97

date

Acknowledgments

The completion of this thesis could not have been accomplished without the inspiration, advice, and support of many people. First and most important, I would like to thank God, because through him alone all things are possible.

I would like to thank my wife, Meg, and my children, Brandi, Sandra, Joseph III, Nicole, and Jared, for their sacrifice during both my undergraduate and graduate studies. It is because of my family that I strive to be the best I can be. I would also like to thank my parents, Patricia and Joseph Sr., to whom I owe everything.

I would like to thank Dr. Victor Bright, my thesis advisor, for expecting nothing less than my complete effort. Also thanks go to the rest of my thesis committee, Major James Lott and Major Donald Gelosh for their words of wisdom and advice.

Thanks also go to the members of the MEMS group, Major Dave Burns, Major Bill Cowan, Captain Jeff Butler, Captain Glen Kading, and Lieutenant Paul Kladitis, who continually supplied alternative ways of approaching a problem.

Table of Contents

	Page
Acknowledgments	ii
Table of Contents	iii
List of Figures	vi
List of Tables.....	x
Abstract	xi
1. Introduction	1-1
1.1. Background	1-1
1.2. Problem Statement	1-3
1.3. Scope	1-4
1.4. Approach	1-5
1.5. Thesis Organization.....	1-7
1.6. References	1-8
2. Literature Review	2-1
2.1. Introduction	2-1
2.2. MEMS Fabrication	2-1
2.3. MUMPS	2-2
2.4. MEMS Devices	2-4
2.4.1. Microhinges.....	2-4
2.4.2. Microlatches	2-5
2.4.3. Microactuators.....	2-6
2.4.4. Fresnel Lens	2-7

	Page
2.4.5. Rotating Mirror	2-8
2.4.6. Fan Mirror	2-9
2.5. VCSELS.....	2-10
2.6. Current Research	2-11
2.7. References	2-13
3. Theoretical Review	3-1
3.1. Introduction	3-1
3.2. VCSEL	3-1
3.3. Fresnel Lens	3-2
3.4. Thermal Actuators.....	3-5
3.5. Mirrors.....	3-6
3.6. Range of Motion.....	3-8
3.7. References	3-10
4. Experimental Setups, Procedures, and Design Descriptions.....	4-1
4.1. Introduction	4-1
4.2. Design Process	4-1
4.3. Design Considerations.....	4-4
4.4. Testing Equipment	4-5
4.5. Test Setups	4-11
4.6. Device Descriptions	4-13
4.6.1. VCSEL Pad	4-13
4.6.2. 135° Mirror	4-15
4.6.3. Fresnel Lens	4-16

	Page
4.6.4. Rotating Mirror	4-18
4.6.5. Fan Mirror	4-21
4.7. References	4-25
5. Results and Discussion.....	5-1
5.1. Introduction	5-1
5.2. Fabrication Results.....	5-1
5.2.1. MUMPs 18	5-3
5.2.2. MUMPs 19	5-6
5.2.3. MUMPs 20	5-8
5.3. Fixing Design Errors with the Laser Cutter	5-10
5.4. VCSEL Operational Characteristics.....	5-13
5.5. VCSEL Bonding.....	5-14
5.5.1. Silver Epoxy Paste Bonding.....	5-15
5.5.2. Solder Bonding.....	5-16
5.5.3. Eutectic Bonding	5-20
5.6. Scanner System Testing	5-22
5.7. References	5-28
6. Conclusions and Recommendations.....	6-1
6.1. Introduction	6-1
6.2. Conclusions	6-1
6.3. Recommendations	6-2
6.4. References	6-7
VITA	VITA-1

List of Figures

Figure	Page
1-1. Evolution of small machines and sensors	1-2
1-2. Beam profiles of (a) an edge-emitting laser, (b) a surface emitting laser	1-3
1-3. Vertical Cavity Surface Emitting Laser	1-5
1-4. Schematic diagram of optical scanner	1-6
2-1. Scanning electron micrograph of (a) Surface micromachined resonant transducer, (b) Bulk micromachined piezoresistive microphone, (c) LIGA gears.....	2-1
2-2. Seven layer MUMPs	2-3
2-3. Basic hinge types. (a) A substrate hinge used to hinge released structures to the substrate. (b) A 'concave down' scissor hinge used to hinge released structures to each other. (c) A 'concave up' scissor hinge	2-5
2-4. Microlatch	2-5
2-5. Thermal microactuator.....	2-6
2-6. Array of heatuators.....	2-7
2-7. Scanning electron micrograph of a micro-Fresnel lens with precision lens mount	2-8
2-8. Scanning electron micrograph of a rotating micromirror	2-8
2-9. Scanning electron micrograph of a fan micromirror.....	2-9
2-10. Schematic diagram of a VCSEL	2-10
2-11. Scanning electron micrograph illustrating UCLA's integration of an edge-emitting laser on a surface-machined MEMS die	2-12
3-1. The laser beam from a VCSEL.....	3-1
3-2. Fresnel zone plates	3-2
3-3. Fresnel zone plate for calculating m^{th} radius	3-3

Figure	Page
3-4. Schematic diagram of (a) single hot arm actuator, (b) double hot arm actuator	3-5
3-5. Triangle formed in the design of (a) fan mirror and (b) rotating mirror	3-6
3-6. Triangle formed in design of 135° mirror	3-8
3-7. Range of motion of the scanner	3-9
4-1. CADENCE layout editor screen of a MEMS scanner system	4-2
4-2. Chemical processing area used to release MEMS devices	4-3
4-3. A cut away view of a flip-up mirror with a substrate hinge.....	4-4
4-4. Micromanipulator station, Model 6200	4-6
4-5. Micromanipulator station, Model LAS-2001.....	4-7
4-6. Scanning electron microscope, Model WB-6	4-8
4-7. Bench top sputter, Model 30800.....	4-8
4-8. Ball bonder, Model 4124	4-9
4-9. Optical power meter, Model FM.....	4-10
4-10. 144 pin chip carrier with a MEMS die mounted and wire bonded	4-11
4-11. Test structure for testing the MEMS die mounted in a 144 pin chip carrier.....	4-12
4-12. CADENCE layout of the VCSEL pad	4-14
4-13. Scanning electron micrograph of VCSEL pad.....	4-14
4-14. CADENCE layout of the 135° mirror	4-15
4-15. Scanning electron micrograph of assembled 135° mirror over a VCSEL bonding pad	4-15
4-16. CADENCE layout of the Fresnel lens	4-17
4-17. Scanning electron micrograph of Fresnel lens	4-17
4-18. Scanning electron micrograph of assembled Fresnel lens	4-18

Figure	Page
4-19. CADENCE layout of the rotating mirror	4-19
4-20. Scanning electron micrograph of rotating mirror.....	4-20
4-21. Scanning electron micrograph of assembled rotating mirror	4-20
4-22. Scanning electron micrograph of rotating mirror's drive mechanism	4-21
4-23. CADENCE layout of the fan mirror	4-22
4-24. Scanning electron micrograph of fan mirror	4-22
4-25. Scanning electron micrograph of assembled fan mirror	4-23
4-26. Scanning electron micrograph of fan mirror's drive mechanism.....	4-23
5-1. MUMPs 18 design layout	5-3
5-2. Scanning electron micrograph of the lock design error on the 135° mirror	5-5
5-3. Scanning electron micrograph of the binding scissor hinge on the 135° mirror	5-5
5-4. MUMPs 19 design layout	5-7
5-5. Scanning electron micrograph of the design error resulting from extending the POLY1_POLY2_VIA mask over Poly 1 layer.....	5-7
5-6. MUMPs 20 design layout	5-8
5-7. Scanning electron micrograph of guide rail before laser cutting	5-10
5-8. Scanning electron micrograph of guide rail after release cut.....	5-11
5-9. Scanning electron micrograph of etch hole cut into the 135° mirror on MUMPs 19	5-11
5-10. Scanning electron micrograph close up of the etch hole on the front side of the mirror	5-12
5-11. Scanning electron micrograph close up of the etch hole on the back side of the mirror	5-12
5-12. The visible band of light	5-13

Figure	Page
5-13. VCSEL operating characteristics	5-14
5-14. Scanning electron micrograph of a VCSEL bonded to a chip carrier using silver epoxy paste	5-15
5-15. Solder placed on a VCSEL pad.....	5-17
5-16. VCSEL pad after solder has flowed.....	5-17
5-17. Scanning electron micrograph of a VCSEL pad with an alignment guide and without a Poly 2 layer on MUMPs 20	5-19
5-18. Scanning electron micrograph of a VCSEL pad with an alignment guide and a Poly 2 layer on MUMPs 20	5-19
5-19. Scanning electron micrograph of a VCSEL bonded onto a MUMPs 19 VCSEL pad	5-20
5-20. Scanning electron micrograph of a VCSEL with a Poly 1 heater on MUMPs 20	5-21
5-21. Scanning electron micrograph of a VCSEL heater pad after soldering and attempting to wire bond a VCSEL	5-22
5-22. Scanning electron micrograph of a complete scanner system assembled MUMPs 20	5-23
5-23. Optical power output of the scanner system	5-26
5-24. Reflectance spectra of gold and silver	5-27
6-1. Beam steering using decentered macroscopic lenses.....	6-2
6-2. Beam steering with the scanning Fresnel lens	6-3
6-3. CADENCE layout of scanning Fresnel lens	6-3
6-4. Scanning electron micrograph of scanning Fresnel lens.....	6-4
6-5. CADENCE layout of MUMPs 21.....	6-5
6-6. Scanning electron micrograph of fan mirror connection points on MUMPs 21..	6-6
6-7. Scanning electron micrograph of assembled fan mirror on MUMPs 21	6-6

List of Tables

Table	Page
4-1. Release Procedure for MUMPs Fabricated Die	4-3
5-1. MCNC Film Data on each MUMPs 18, 19, and 20.....	5-2

Abstract

Optical scanners play a prominent role in the commercial and military industries. The scanner's size, cost and reliability are critical characteristics. In this research a micro-optical scanning system was fabricated by incorporating a vertical cavity surface emitting laser (VCSEL) onto a surface-machined microelectromechanical die. The micro optics for laser beam steering includes a 135° mirror, a Fresnel lens, a lateral scanning rotating mirror, and a vertical scanning fan mirror. The VCSEL was attached to the die by solder and electrical connection was provided by wire bonding. Based on far field measurements the scanner had a lateral scan angle of 5.7 degrees and a vertical scan angle of 4.4 degrees. Based on spot diameter measurements at the fan mirror the scanner had a divergence angle of 0.524 degrees. The potential military applications of these scanners include laser radars, laser detectors, holographic storage devices, and data links between integrated circuit chips.

Microelectromechanical Scanner Using a Vertical Cavity Surface Emitting Laser

Chapter 1

Introduction

1.1 Background

Micro-Electro-Mechanical Systems (MEMS) development over the past ten years has made remarkable progress. MEMS have many advantages including miniaturization, multiple components, microelectronics [1], and the ability to be mass produced using conventional microfabrication techniques. MEMS consist of miniaturized electrical and mechanical components. The electronic components enable data processing, while the mechanical components provide an interface between the electronics and the physical world. Figure 1-1 shows the relationship between the electronic and mechanical components. The vertical axis shows the number of transistors, which is roughly proportional to processing ability. The horizontal axis shows the number of mechanical components, which is a measure of the devices' ability to sense and control motion, light, sound, heat and other physical quantities.

Optical MEMS, or Micro-Opto-Electro-Mechanical Systems (MOEMS) [4], combines microactuators, microsensors, and integrated micro optics into a complete optical system that fits on a single chip. MOEMS dates back to 1977 when small cantilevers, driven by electrostatic forces, reflected light beams [5]. Since then, three-dimensional hinged structures have been developed to facilitate the realization of micro-optical scanners.

Trends in Microelectromechanical Systems

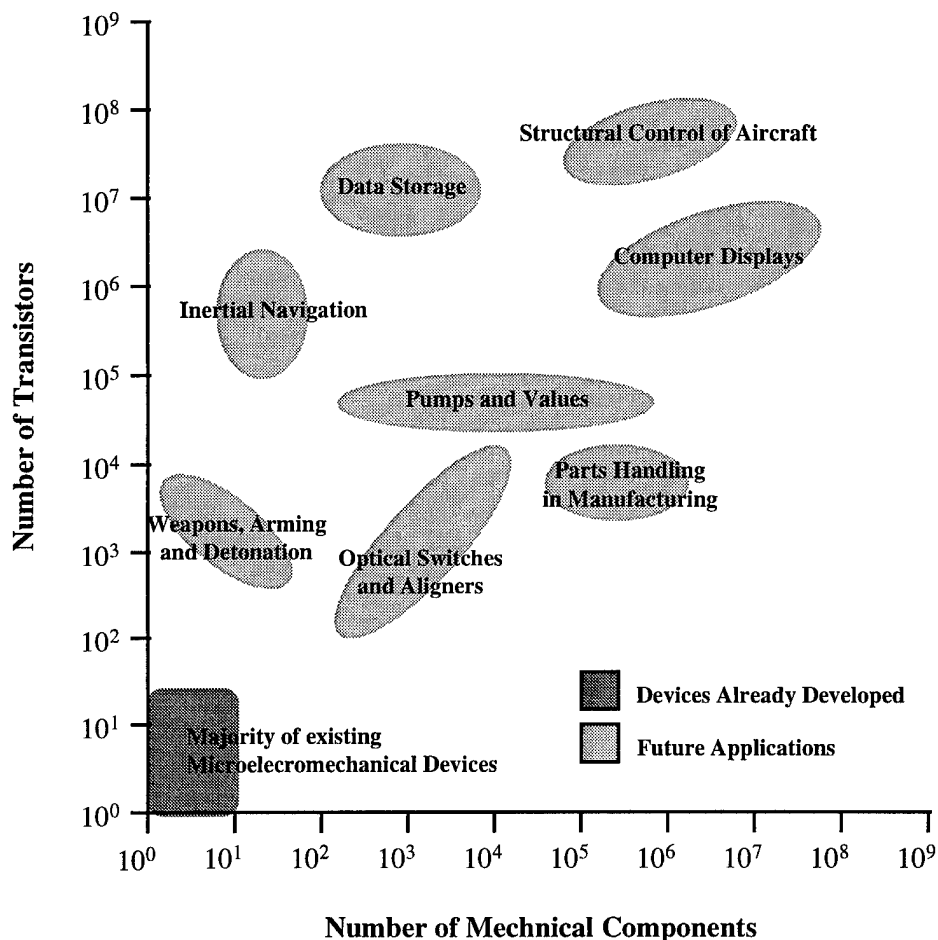


Figure 1-1. Evolution of small machines and sensors [2, 3].

Optical scanners have long been used by the commercial and military industries where the ultimate goal is to increase the reliability and reduce the size and cost. By combining MEMS with semiconductor lasers, entire optical scanners can be made on single surface-machined silicon dies.

Optical scanning applications include bar-code reading, graphic arts, image digitizing, quality control inspections, data storage, printing, pattern generation, and medical imaging [6]. Additional optical scanning applications include laser radars, optical

communications [7], laser-guided weapons, and laser sensors. Potential future applications include holographic storage devices [8] and intrachip data-links [9].

Previous MEMS optical scanner designs have used an off chip laser source or incorporated an edge-emitting laser. Edge-emitting lasers have an inherent drawback. The emitted beam has an asymmetrical pattern, which usually requires additional optics to correct the beam back into circular shape. Vertical Cavity Surface Emitting Lasers (VCSELs) on the other hand are more desirable due to their low threshold current, circular beam pattern and small beam divergence [10]. The edge-emitting laser and VCSEL are depicted in Figure 1-2.

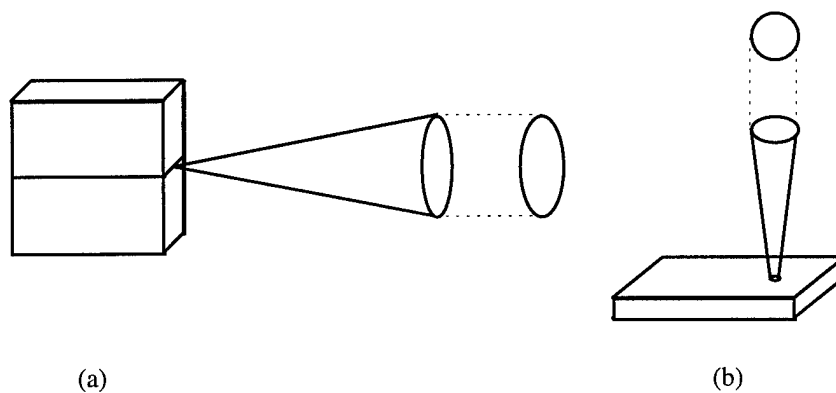


Figure 1-2. Beam profiles of (a) an edge-emitting laser, (b) a surface emitting laser.

1.2 Problem Statement

The Department of Defense has identified three major application areas for MEMS: 1) inertial measurements; 2) distributed sensing and control; and 3) information technology [11]. Optical scanning applies in each of the three areas, for example smart munitions, identify-friend or foe systems, and mass storage devices respectively. In addition, the Department of Defense has initiated the near-term challenge of developing

materials, processes, and devices for the integration of 1,000 mechanical components/cm² with on-chip electronics of at least 10,000 transistors [12].

Now that VCSELs are commercially available, the evolution of optical scanners can continue. The United States Air Force can benefit from this technology through potential applications in laser-guided weapons, laser radars, and laser detectors. The integration of a VCSEL and a MEMS die could allow development of an automated process for the fabrication of VCSEL-based micro scanners.

1.3 Scope

This research covers the design, fabrication and testing of a MEMS optical scanner based on a VCSEL light source. The MEMS die was designed by using the CADENCE layout software design tool package. This software is installed on the Center for Advance VLSI Research's computer network. Several previous device designs, after slight modification, were used in the MEMS optical scanner including: the rotating mirror, Fresnel lens, fan mirror and microhinges.

The MEMS devices that provide laser beam steering are fabricated by surface-machined MEMS. The Air Force Institute of Technology (AFIT) uses the Defense Advanced Research Projects Agency (DARPA) sponsored program provided by MCNC, Inc., which provides the Multi-User MEMS Processes (MUMPs) [13].

Testing of the MUMPs fabricated devices and mounting the VCSEL onto the die were accomplished through the use of equipment in the AFIT Cooperative Microelectronics Laboratory in Building 125 and the Photonics Research Laboratory in Building 194.

1.4 Approach

The approach for this thesis is to design, fabricate, and demonstrate an optical scanning device using a VCSEL integrated onto a MEMS optical bench. The VCSELs obtained for this research are based on gallium arsenide. The VCSELs consists of alternating layers of gallium arsenide and aluminum gallium arsenide. The dimensions for the VCSEL chip are approximately 600 μm long by 300 μm wide by 100 μm high. The circular aperture for the VCSEL is 8 to 10 μm in diameter and located approximately in the center of the device. Figure 1-3 shows the physical layout of the VCSEL. The VCSEL lases by

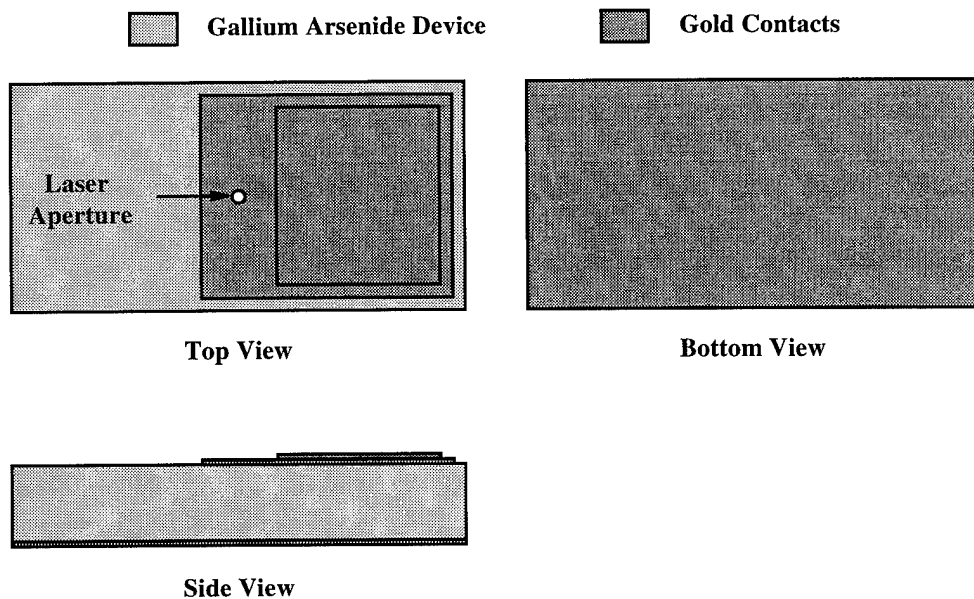


Figure 1-3. Vertical Cavity Surface Emitting Laser.

applying a positive voltage (approximately 3.3 volts) to the top contact and ground to the bottom contact. The top contact consists of two gold pads. The first gold pad, adhered to the gallium arsenide by thin layer of titanium, makes electrical contact with the device

and contains the laser aperture. The second gold pad, which is much thicker than the first, is used as a bonding pad.

Figure 1-4 shows the schematic diagram for the design of the optical scanner. The

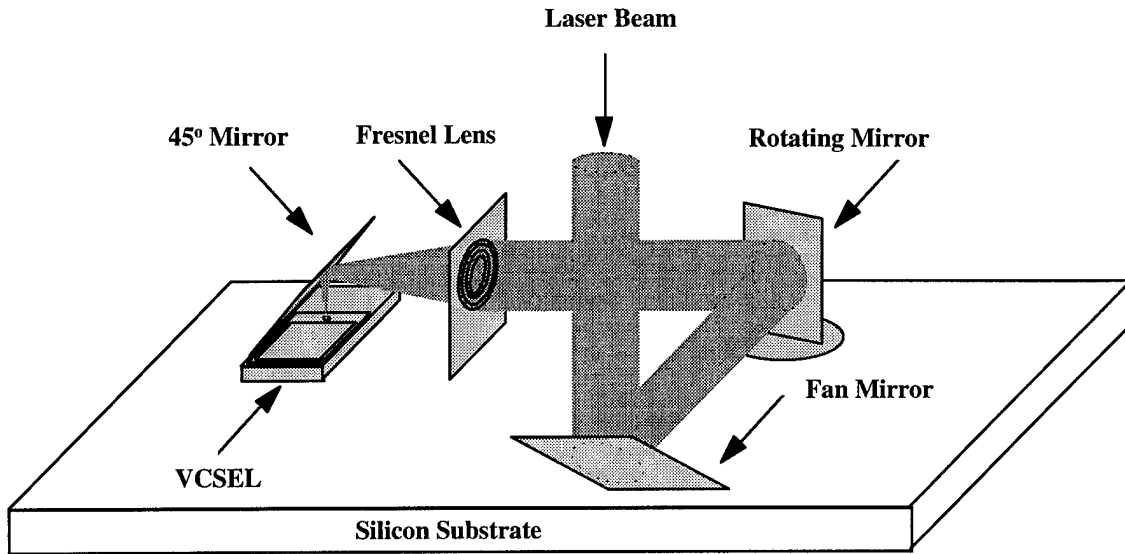


Figure 1-4. Schematic diagram of optical scanner.

design of the optical scanner will start with a surface-machined MUMPs die. The VCSEL will be placed into a small depression created in the substrate in the MUMPs die. Several optical devices are required to allow the VCSEL's beam to be scanned. A mirror will be placed over the VCSEL at a 45° angle. The laser beam from the VCSEL, which is normal to the surface of the wafer, will hit the mirror and be reflected 90° resulting in a beam parallel to the surface of the wafer. The beam will then pass through corrective optics and a Fresnel lens will collimate the beam. A rotating or pivoting mirror will be used next to laterally scan the laser beam. The final optical device will be a fan mirror, which will allow the beam to scan vertically and reflect the beam normal to the surface of the wafer.

1.5 Thesis Organization

This thesis consists of six chapters. Chapter 2 gives a detailed description of MUMPs and previous MEMS devices, which can be modified and used in the fabrication of the optical scanner. Also discussed in Chapter 2 is the operation of VCSELs, and a review of the efforts of other researchers. The theory behind the MEMS optical devices used in the optical scanner is presented in Chapter 3. Chapter 4 describes the experimental setup and procedures used to test each device. Chapter 4 also gives a full description of each MEMS fabricated device used in the optical scanner. Chapter 5 shows the results of the tests performed on each device. Chapter 6 contains the conclusions and recommendations with emphasis on further research areas to expand on this thesis.

1.6 References

- [1] H. Fujita, "Application of micromachining technology to optical devices and systems," *Proc. SPIE*, vol. 2879, pp. 2-11, October 1996.
- [2] K. J. Gabriel, "Engineering microscopic machines," *Scientific American*, pp. 150-3, September 1995.
- [3] K. J. Gabriel, "Microelectromechanical systems," *1997 IEEE Aerospace Conference Proceedings*, Aspen, CO., pp. 9-43, February 1-8, 1997.
- [4] V. M. Bright, J. H. Comtois, D. E. Sene, J. R. Reid, S. C. Gustafson and E. A. Watson, "Realizing micro-opto-electro-mechanical devices through a commercial surface-micromachining process," *Proc. SPIE*, vol. 2687, pp. 34-46, January 1996.
- [5] K. E. Petersen, "Micromechanical light modulator array fabricated on silicon," *Applied Physics Letters*, vol. 31, no. 8, pp. 521-3, October 1977.
- [6] M. E. Motamedi, S. Park, A. Wang, M. S. Dadkhah, A. P. Andrews, H. O Marcy, M. Khoshnevisan, A. E. Chiou, R. J. Huhn, C. F. Sell and J. G. Smits , "Development of micro-electro-mechanical optical scanner," *Optical Engineering*, vol. 36, no. 5, pp. 1346-53, May 1997.
- [7] M. E. Motamedi, A. P. Andrews, W. J. Gunning and M. Khoshnevisan, "Miniaturized micro-optical scanners," *Optical Engineering*, vol. 33, no. 11, pp. 3616-23, November 1994.
- [8] R. A. Miller and Y. Tai, "Micromachined electromagnetic scanning mirrors," *Optical Engineering*, vol. 36, no. 5, pp. 1399-1407, May 1997.
- [9] M. R. T. Tan, Y. M. Houn, K. H. Hahn, A. G. Weber, S. Y. Wang and K. W. Carey, "VCSELs for short distance data links," *IEEE Lasers and Electro-Optics Society 1995 Conference Proceedings*, San Francisco, CA., vol. 1, pp. 107-8, October 30-31, 1995.
- [10] J. Jewell and G. Olbright, "Arrays of vertical cavity surface-emitting lasers go commercial," *Optics and Photonic News*, vol. 5, no. 3, pp. 8-11, March 1994.
- [11] "Microelectromechanical Systems," *A DoD Dual use Technology Industrial Assessment Final Report*, p. 4, December 1995.
- [12] *Defense Technology Area Plan*, Director of Defense Research and Engineering, Section II, par. SE.38.01, pp. II-159, January 1997.

- [13] D. A. Koester, R. Mahadevan, A. Shishkoff and K. W. Markus, " SmartMUMPs Design Handbook including MUMPs Introduction and Design Rules (rev. 4)," MCNC Internet website, <http://mems.mcnc.org/smumps/SMTOC.html>, MEMS Technology Application Center, MCNC, NC, 1996.

Chapter 2

Literature Review

2.1 Introduction

Oscillatory (or galvanometric) optical scanners have been around for well over a century. Galvanometric scanners use mirrors as beam deflectors to electronically steer a reflected beam onto a target [1]. There are numerous ways to design the components of an optical scanner using MEMS. This chapter will look at the processes currently used to fabricate MEMS devices, basic surface machined devices, VCSELs, and current research being accomplished in this field.

2.2 MEMS Fabrication

MEMS devices are fabricated by three methods: surface micromachining, bulk micromachining, and LIGA [2]. Examples of devices produced by the three MEMS fabrication methods are shown in Figure 2-1.

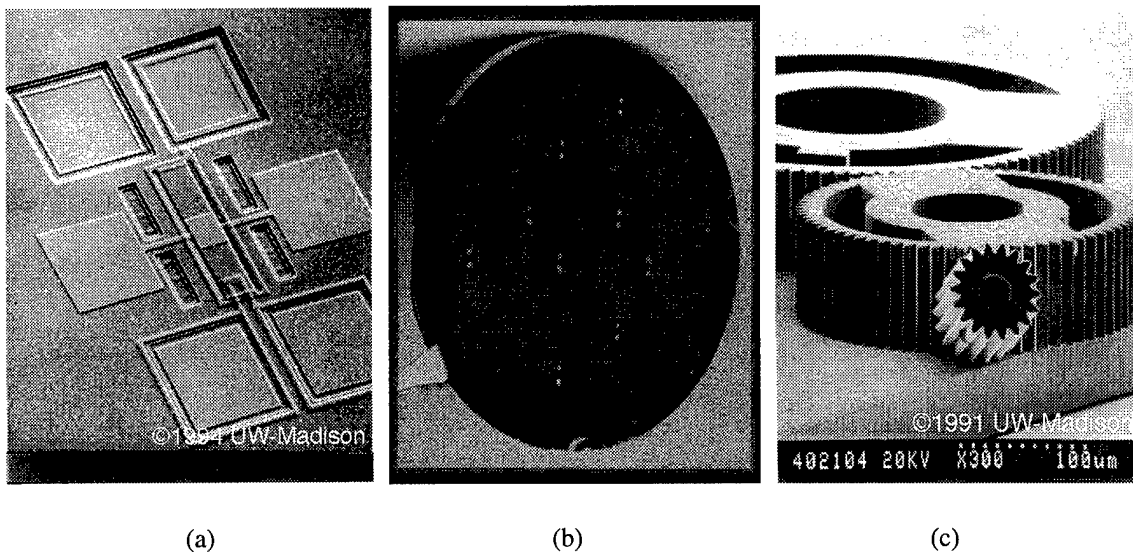


Figure 2-1. Scanning electron micrographs of (a) Surface micromachined resonant transducer, (b) Bulk micromachined piezoresistive microphone, and (c) LIGA gears [3].

The LIGA process forms high-aspect ratio structures through the use of polymer molds and electroplating. Photolithography and exposure to X-ray or ultraviolet radiation form the polymer molds. Metal electroplating then forms the device in the polymer mold, which can be used over and over.

Bulk micromachining is a process of etching devices in a bulk silicon wafer. Etching is accomplished by either exposing the wafer to a wet chemical etchant that is orientation or concentration dependent when applied to silicon, or a dry etchant, typically a Reactive Ion Etch (RIE).

The final method, surface micromachining, is a process of depositing alternate layers of polysilicon and oxide onto a silicon wafer. The polysilicon layers are patterned and etched, while the oxide layers are sacrificial layers that are subsequently removed.

2.3 MUMPS

The micro-optics required to provide beam steering of the laser are fabricated by surface-machined MEMS. The Air Force Institute of Technology (AFIT) uses the Defense Advanced Research Projects Agency (DARPA) sponsored program that provides the Multi-User MEMS Processes (MUMPs) [4].

MUMPs is a seven-layer process that uses three layers of polysilicon. The process begins with an n-type silicon wafer with a <100> orientation. First, the surface of the wafer is highly doped with phosphorus (10^{20} cm^{-3} , about 0.5 μm deep) to prevent charge feedthrough to the substrate from devices fabricated on the surface. A silicon nitride layer is deposited to provide electrical isolation. Each additional layer is deposited, patterned, and etched before the next layer is deposited. A photoresist mask and reactive

ion etching are used to pattern the polysilicon and oxide layers. Figure 2-2 shows the order of the layers used in MUMPs and their thickness. To pattern the metal layer a

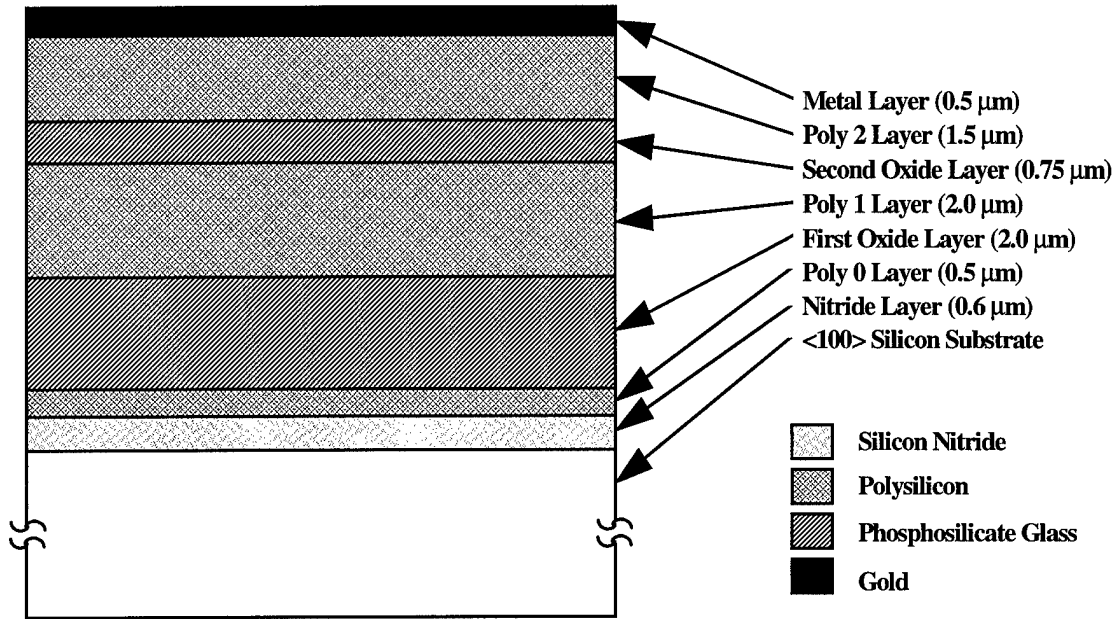


Figure 2-2. Seven layer MUMPs.

photoresist mask and the lift-off technique are used. Finally the completed wafer is covered with photoresist to protect the devices, diced into chips, and shipped to the user.

In addition to patterning the polysilicon layers, MUMPs provides four other photoresist masks and RIE etching of oxide layers. The first oxide layer, if desired, can have a DIMPLE and an ANCHOR 1 mask. Dimples, which are placed under the releasable polysilicon layers, help prevent the polysilicon layers from adhering to the substrate or to another polysilicon layer. The depth of the dimples is 750 nm. A Poly 1 anchor enables the Poly 1 layer to be secured to the Poly 0 or Nitride layer. The Poly 1 anchor prevents Poly 1 devices from washing away during the release etch. The second oxide layer, if desired, can have a POLY1_POLY2_VIA and an ANCHOR 2 mask. The

POLY1_POLY2_VIA etch provides etch holes which enable mechanical and electrical connection between the Poly 1 and Poly 2 layers. The ANCHOR 2 etch provides etch holes through both oxide layers which enables the Poly 2 layer to be secured to the Poly 0 or Nitride layer. The Poly 2 anchor prevents Poly 2 devices from washing away during the release etch.

2.4 MEMS Devices

The three-dimensional structures developed through surface micromachining use microhinges, microlatches, and microactuators. These assemblies enable surface-machined parts to be rotated out of the plane of the wafer, latched into position, and moved to a desired angle.

2.4.1 Microhinges

The microhinges are divided into substrate (or staple) hinges and scissor hinges [5]. The substrate hinge consists of a Poly 1 plate and hinge pin and a Poly 2 staple over the hinge pin. The Poly 2 staple is anchored to the nitride layer on both sides of the Poly 1 hinge pin. A scissor hinge can connect two Poly 1 plates or two Poly 2 plates. The design of the scissor hinge allows the structure to be either concave up or concave down.

A third hinge, called a floating substrate hinge [6], is a modification of the substrate hinge allowing the hinged structures to move across the surface of the substrate. This is accomplished by anchoring a Poly 2 staple to a Poly 1 plate by a POLY1_POLY2_VIA. The floating substrate hinge is used in the design of the rotating mirror discussed later in this chapter. The designs of the basic hinge types are shown in Figure 2-3.

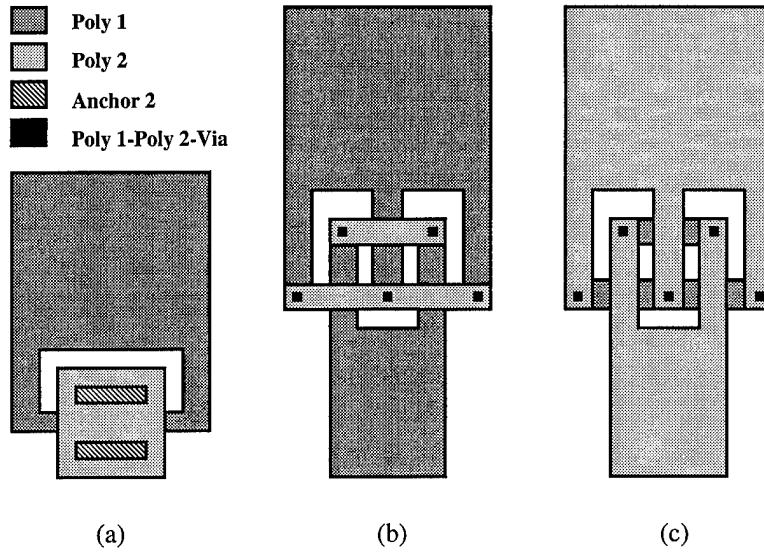


Figure 2-3. Basic hinge types. (a) A substrate hinge used to hinge released structures to the substrate. (b) A 'concave down' scissor hinge used to hinge released structures to each other. (c) A 'concave up' scissor hinge.

2.4.2 Microlatches

Microlatches allow structures to be latched into a position with a specific angle relative to the surface of the wafer. Figure 2-4 shows the design layout of a microlatch [7].

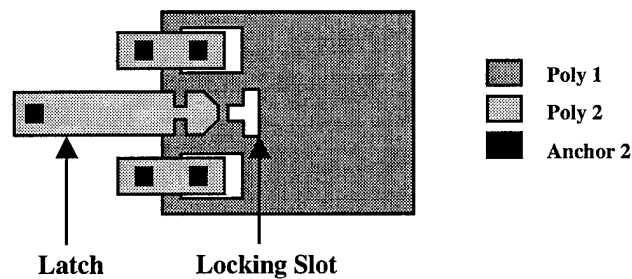


Figure 2-4. Microlatch.

When the device is raised into position, the microlatch moves along the surface of the device until it drops into position in the locking slot.

2.4.3 Microactuators

There are numerous types of microactuators, but the most common are electrostatic, thermal, and magnetic. Electrostatic actuators, like the comb-actuator [8] and the scratch drive actuator [9], use a voltage difference between two plates to create an electrostatic force. However, the electrostatic force decreases with increasing plate separation, increasing the device operation voltages. The voltage may exceed 100 volts and is thus not compatible with standard integrated circuit electronics.

Magnetic actuators require a magnetic material to be incorporated into the MEMS die [10]. This normally requires bulk micromachining to remove the substrate below the device, such as a micromirror, followed by the addition of a layer of magnetic material. By applying an external magnetic field, again not compatible with standard integrated circuit electronics, actuates the device.

A thermal actuator (or heatuator) is a polysilicon device. An example of a thermal actuator is shown in Figure 2-5 [11]. The only requirement in designing the heatuator

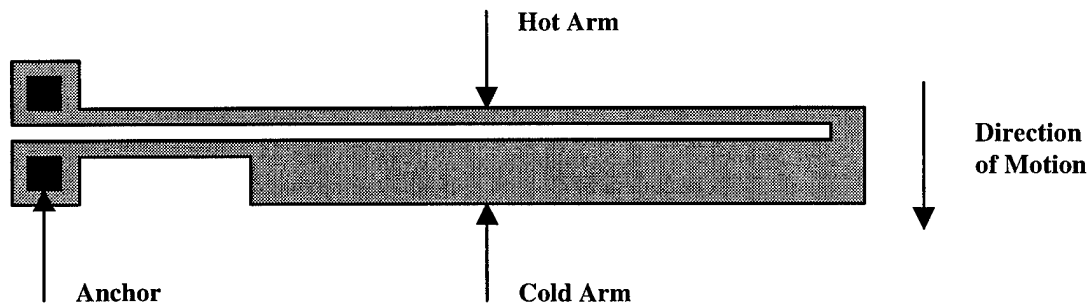


Figure 2-5. Thermal microactuator.

is that the hot arm must expand more than the cold arm. When current is applied to the heatuator a higher current density in the hot arm causes it to heat and expand more than

the wider cold arm. Removing the current from the heatuator returns it to its normal state provided the actuator does not deform due to excessive heating. A lateral arcing motion is allowed when the current is alternately applied and removed from the heatuator. Several of the heatuators can be combined to form an array to provide enough force to move a MEMS device. An array of heatuators is shown in Figure 2-6. The array is connected to a yoke. The yoke is connected to the tether, which transfers the force to a device.

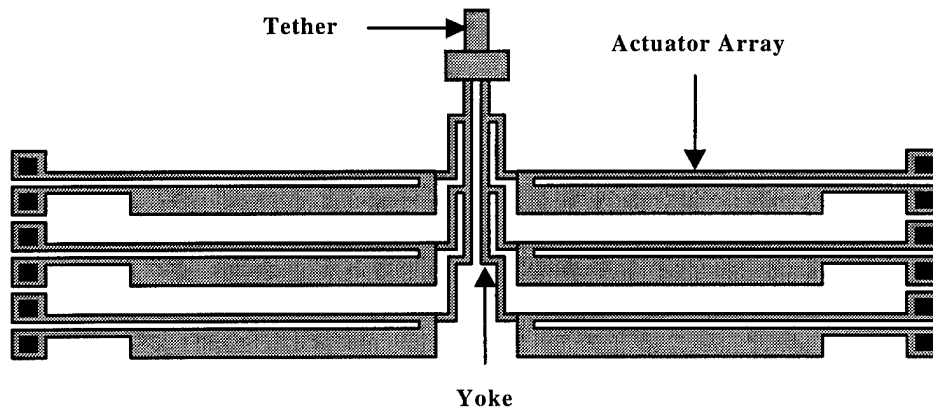


Figure 2-6. Array of heatuators.

2.4.4 Fresnel Lens

The laser beam from a circular aperture device, the VCSEL for example, tends to diverge and requires focusing optics. In macro systems curved refractive lenses are used, but due to the limitations of surface micromachining curved lenses are not possible [12]. Fresnel lenses can be easily fabricated using a surface micromachining process and have been used to focus and collimate diverging beams of light from laser diodes, optical fibers, edge-emitting lasers, and surface emitting lasers. Figure 2-7 shows a surface

micromachined micro-Fresnel lens, which has a diameter of 280 μm and an optical axis 254 μm above the surface of the die [13].

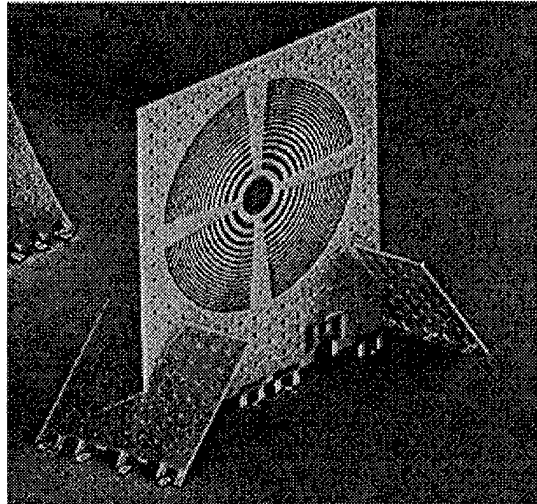


Figure 2-7. Scanning electron micrograph of a micro-Fresnel lens with precision lens mount [13].

2.4.5 Rotating Mirror

Steering a beam of light parallel to the surface of the substrate is possible using a surface machined rotating micromirror [6]. The rotating mirror, shown in Figure 2-8, is made up of three parts: a flip-up optical mirror, a rotating circular plate, and a thermal

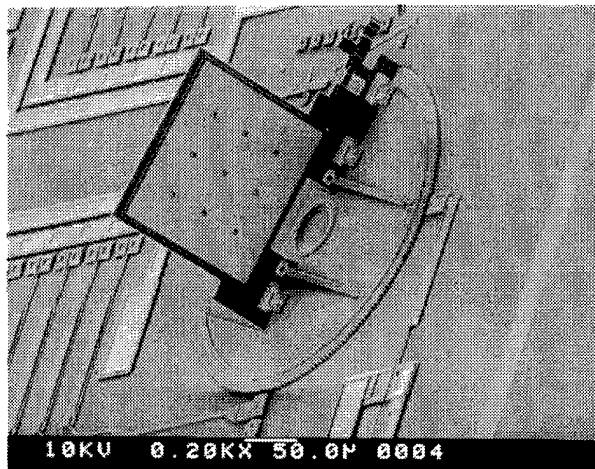


Figure 2-8. Scanning electron micrograph of a rotating micromirror [6].

actuator drive system. The Poly 1 circular plate is anchored to the substrate with a Poly 2 circular anchor, which overlaps the circular plate, allowing the circular plate to rotate around the anchor. The mirror is attached to the circular plate by the use of floating substrate hinges and locked into place by microlatches. Motion of the mirror is provided by the thermal actuator drive system. This system is made of three parts: a single actuator to lock the circular plate, a single actuator to engage the drive arm, and an array of actuators that provides lateral motion to the drive arm. The drive system can provide motion in both directions.

2.4.6 Fan Mirror

Steering a beam of light normal to the surface of the substrate is possible using a surface machined scanning micromirror, or fan mirror [7]. The fan mirror, shown in Figure 2-9, is made up of three parts: a flip-up optical mirror, a self-locking tether, and a thermal actuator array. The mirror is anchored to the substrate by the use of substrate

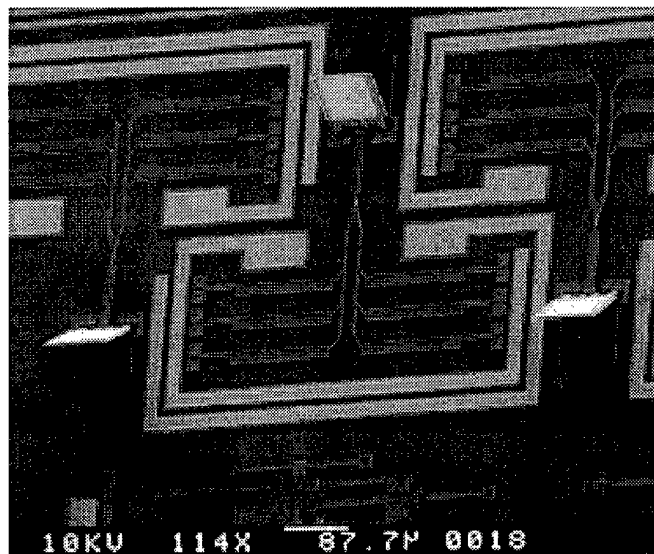


Figure 2-9. Scanning electron micrograph of a fan micromirror [7].

hinges. The mirror is locked into place by the self-locking tether. The self-locking tether is based on the microlatch design, but is attached to the yoke of the actuator array instead of being anchored. The actuator array provides the lateral motion to allow the mirror to rotate about the pin arm of the substrate hinge.

2.5 VCSELs

Laser theory can be traced back to the early 1900's with Einstein's atomic theories. The first semiconductor laser was demonstrated in 1962 [14]. The first low-threshold VCSEL was produced in 1989 [15]. VCSELs are fabricated using photolithography and epitaxial growth, which allows the higher uniformity between devices compared to edge-emitting lasers. Figure 2-11 shows the schematic representation of a VCSEL. The active region consists of one or more quantum well(s) sandwiched between undoped barrier

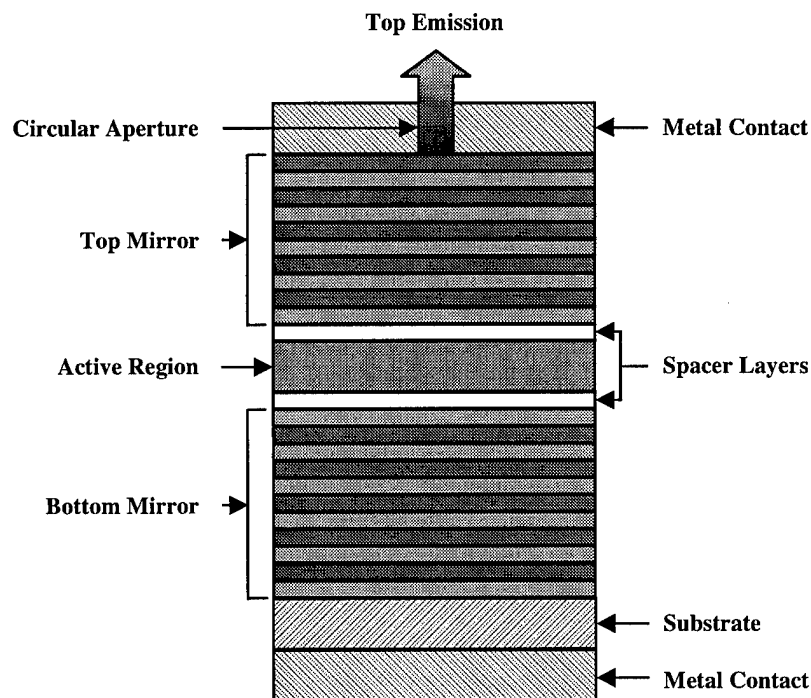


Figure 2-10. Schematic diagram of a VCSEL.

layers. The active region is sandwiched between two spacer layers, which in turn are sandwiched between n-type and a p-type distributed Bragg mirrors. The Bragg mirrors consist of alternating quarter-wave layers of low and high refractive index material. The thickness of the optical layers is equal to a quarter of the wavelength of the output light. The layer of metal used on the top and bottom of the VCSEL provide electrical contacts.

Confining the electrical current and optical field from the sides of the VCSEL is accomplished by either gain guiding or index guiding [16]. Gain guiding confines the electrical current by blocking off the rest of the device with insulating layers. The insulating layers can be obtained by ion implantation. Index guiding surrounds the sides of the active region with a material with a different refractive index.

2.6 Current Research

The University of California Los Angeles (UCLA) is working on a free-space micro-optical bench for integrating optics [17]. UCLA's design uses a self-aligning structure to mount the laser and side-latches to align the Fresnel lens. The laser is placed between two contact pads and conductive silver epoxy is applied to make electrical contact. This is shown in Figure 2-12, including the incorporation of an edge-emitting laser.

UCLA has also incorporated VCSELs into a MEMS die [19]. They took an 8X1 array of VCSELs and mounted it perpendicular to the substrate using the same technique employed to mount the edge-emitting laser. The VCSELs aligned with an 8X1 array of Fresnel lenses, which collimated the laser beams. This setup is used for connection with an array of optical fibers.

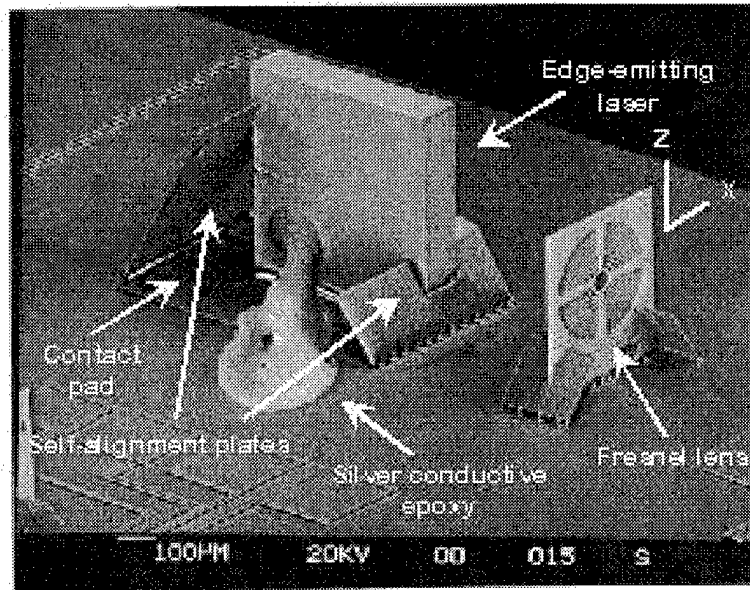


Figure 2-11. Scanning electron micrograph illustrating UCLA's integration of an edge-emitting laser on a surface-machined MEMS die [18].

The latest work by UCLA involves a two-dimensional scanning microlens for VCSELs [20]. The scanning microlens design is a “doubly folded” polysilicon plate, which positions the microlens over a VCSEL. The scanning microlens is a diffractive Fresnel lens and is driven by an electrostatic scratch drive actuator. This scanner provides a 16° scanning range with a resolution of 0.002° .

2.7 References

- [1] G. F. Marshall and J. Montagu, "Advances in oscillatory optical scanners," *Proc. SPIE*, vol. 2383, pp. 440-448, February 1995.
- [2] K. Najafi, "Silicon micromachining technologies: future needs and challenges," *Proc. SPIE*, vol. 2879, pp. 206-215, October 1996.
- [3] Picture downloaded from University of Wisconsin's Internet website, <http://mems.engr.wisc.edu/images>, August 1997.
- [4] D. A. Koester, R. Mahadevan, A. Shishkoff and K. W. Markus, "SmartMUMPs Design Handbook including MUMPs Introduction and Design Rules (rev. 4)," MCNC Internet website, <http://mems.mcnc.org/smumps/SMTOC.html>, MEMS Technology Application Center, MCNC, NC, July 1996.
- [5] K. S. J. Pister, M. W. Judy, S. R. Burgett and R. S. Fearing, "Microfabricated hinges," *Sensors and Actuators A*, vol. 33, pp. 249-256, June 1992.
- [6] J. R. Reid, V. M. Bright and J. H. Comtois, "A surface micromachined rotating micro-mirror normal to the substrate," *IEEE LEOS Summer Topical Meeting*, pp. 39-40, August 7-9, 1996.
- [7] J. R. Reid Jr., "Microelectromechanical isolation of acoustic wave resonators," *Doctoral Dissertation*, Air Force Institute of Technology, Wright-Patterson AFB, Ohio, AFIT/DS/ENG/96-12, December 1996.
- [8] N. C. Tien, M. H. Kiang, M. J. Daneman, O. Solgaard, K. Y. Lau and R. S. Muller, "Actuation of polysilicon surface-micromachined mirrors," *Proc. SPIE*, vol. 2687, pp. 53-59, January 1996.
- [9] T. Akiyama and H. Fujita, "A quantitative analysis of scratch drive actuator using buckling motion," *Proc. IEEE MEMS 1995*, pp. 310-315, January 29-February 2, 1995.
- [10] R. A. Miller and Y. C. Tai, "Micromachined electromagnetic scanning mirrors," *Optical Engineering*, vol. 36, no. 5, pp. 1399-1407, May 1997.
- [11] J. R. Reid, V. M. Bright and J. H. Comtois, "Arrays of thermal micro-actuators coupled to micro-optical components," *Proc. SPIE*, vol. 2865, pp. 74-82, August 1996.

- [12] V. M. Bright, J. H. Comtois, J. R. Reid, and D. E. Sene, "Surface micromachined mirco-opto-electro-mechanical systems," *IEICE Transactions on Electronics*, vol. E80-C, no. 2, pp. 206-213, February 1997.
- [13] M. C. Wu, L. Y. Lin, and S. S. Lee, "Micromachined free-space integrated optics," *Proc. SPIE*, vol. 2291, pp. 40-51, July 1994.
- [14] M. Henini, "A new breed of diode lasers: surface emitting lasers," *III-Vs Review*, vol. 9, no. 4, pp. 37-41, August 1996.
- [15] J. Jewell and G. Olbright, "Arrays of vertical cavity surface-emitting lasers go commerical," *Optics & Photonics News*, vol. 5, no. 3, pp. 8-11, March 1994.
- [16] E. J. Lerner, "Laser diodes and LEDs light optoelectric devices," *Laser Focus World*, vol. 33, no. 2, pp. 109-117, February 1997.
- [17] M. C. Wu, L. Y. Lin, S. S. Lee, and K. S. J. Pister, "Micromachined free-space integrated micro-optics," *Sensors and Actuators A*, vol. 50, pp. 127-134, 1995.
- [18] Picture downloaded from UCLA's Internet website, <http://www.janet.ucla.edu/stdnt.rsrch/pictures>, March 1997.
- [19] S. S. Lee, L. Y. Lin, K. S. J. Pister, M. C. Wu, H. C. Lee and P. Grodzinski, "Passively aligned hybrid integration of 8 X 1 micromachined micro-fresnel lens arrays and 8 X 1 vertical-cavity surface-emitting laser arrays for free-space optical interconnect," *IEEE Photonics Technology Letters*, vol. 7, no. 9, pp. 1031-1033, September 1995.
- [20] L. Fan, M. C. Wu, and K. D. Choquette, "Two-dimensional scanning microlenses for vertical-cavity surface-emitting lasers," *CLEO '97*, pp. 19-20, May 18-23, 1997.

Chapter 3

Theoretical Review

3.1 Introduction

This chapter includes the development and explanation of the mathematical descriptions of the devices used in this thesis. These derived equations provide a theoretical basis for the development of the MEMS devices and are used for comparison with the experimental data collected from the fabricated devices in Chapter 5. This chapter contains a review of the theories of VCSEL beam emission, the Fresnel lenses, thermal actuators, and micro mirrors used in the MEMS scanner.

3.2 VCSEL

The VCSELs used in this research, described in Chapter 1, have an aperture diameter of 5 to 10 microns. The VCSELs also have a full angle beam divergence of 8 to 10 degrees. With this information, the diameter of the beam can be determined at any given distance from the VCSEL. Referring to Figure 3-1, the dimensions of the aperture

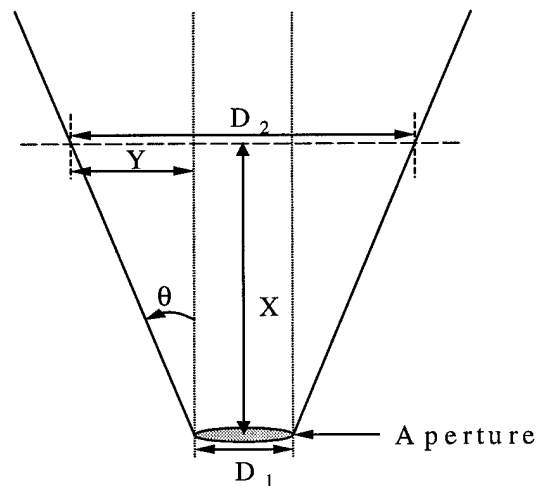


Figure 3-1. The laser beam from a VCSEL.

diameter, D_1 , and the half divergence angle, θ , are known values. At any given distance, X , from the aperture a right triangle is formed with θ and the divergence distance Y . By using plane trigonometry for a right triangle,

$$\tan \theta = \frac{Y}{X}. \quad (3.1)$$

The diameter of the beam, D_2 , at any given distance, X , is given by

$$D_2 = D_1 + 2(Y). \quad (3.2)$$

Therefore, in the worst case ($D_1 = 10 \mu\text{m}$ and $\theta = 10^\circ$), the diameter of the beam at a distance of $500 \mu\text{m}$ from the aperture is equal to $186.3 \mu\text{m}$.

3.3 Fresnel Lens

A Fresnel lens is an optical device used to focus a light source. By using a set of concentric circular zones, shown in Figure 3-2, light can be focused [1].

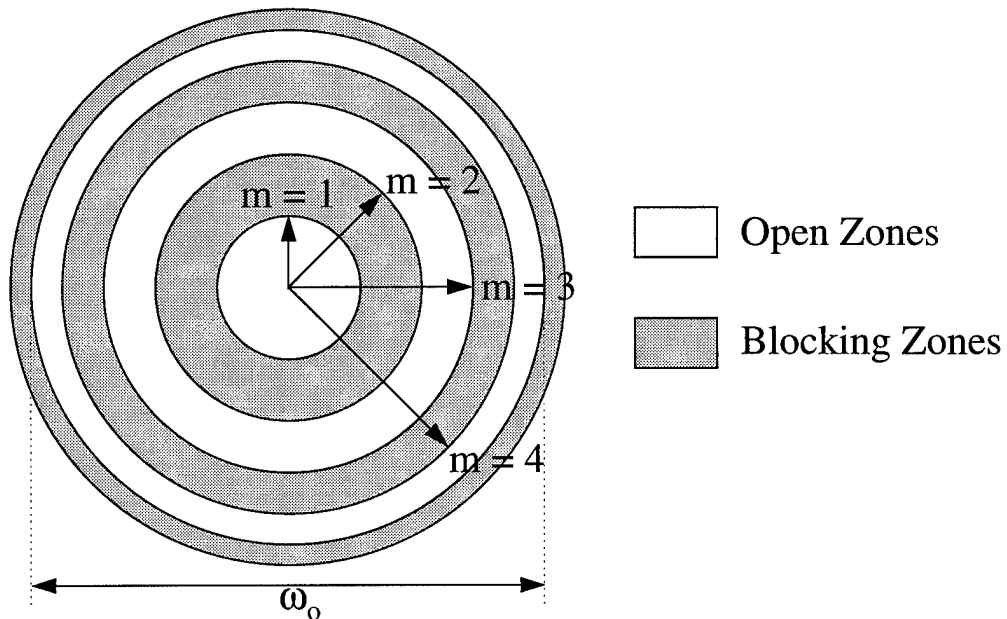


Figure 3-2. Fresnel zone plates.

The width and radius of the circular zones are chosen so that the light passing through the open zones has a path difference of λ with adjacent open zones and a path difference of $\lambda/2$ with adjacent closed zones [2]. The path difference in the open zones, see Figure 3-3, is

$$(R + P) - (R_o + P_o) = m\lambda \quad (3.3)$$

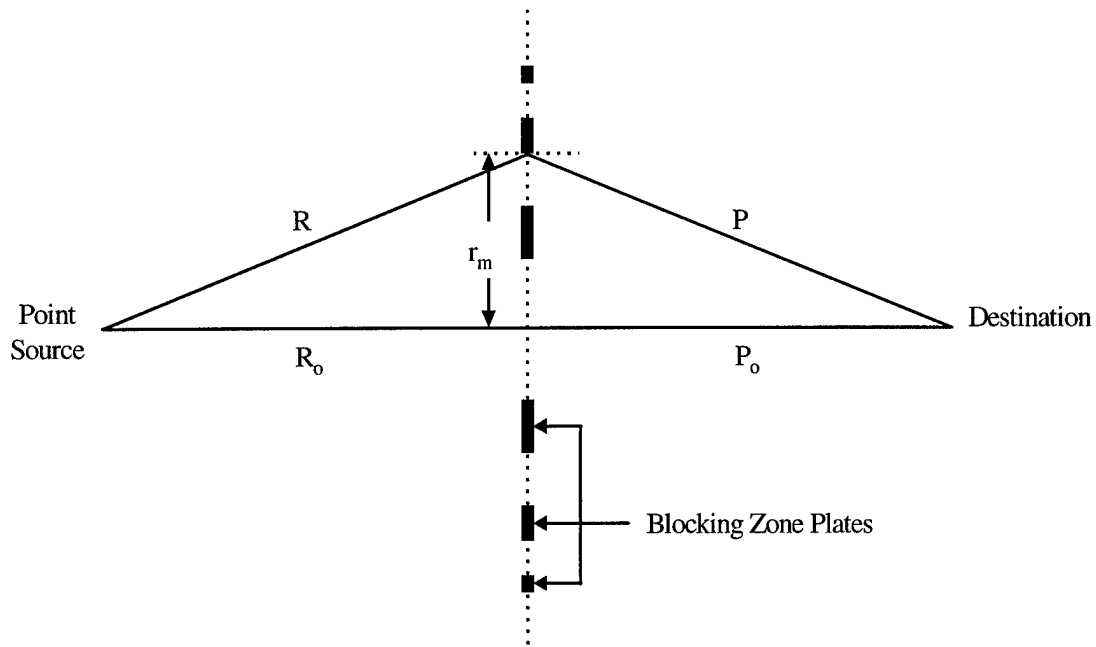


Figure 3-3. Fresnel zone plate for calculating m^{th} radius [2].

where $m = 1, 2, 3, \dots$ and λ is the wavelength of the laser. The path difference in the blocking zones is

$$(R + P) - (R_o + P_o) = \frac{m\lambda}{2} \quad (3.4)$$

The radius of the m^{th} blocking zone is

$$r_m = P^2 - P_o^2 = R^2 - R_o^2 \quad (3.5)$$

Because r_m is small compared to R and P , R and P can be approximated using the first two terms of a binomial series expansion producing

$$P = \sqrt{P_o^2 + r_m^2} \cong P_o \left[1 + \frac{1}{2} \left(\frac{r_m^2}{P_o^2} \right) \right] \quad (3.6)$$

$$R = \sqrt{R_o^2 + r_m^2} \cong R_o \left[1 + \frac{1}{2} \left(\frac{r_m^2}{R_o^2} \right) \right]. \quad (3.7)$$

Taking the results of Equations 3.6 and 3.7 and inserting them back into Equation (3.4) yields

$$R_o + \frac{1}{2} \left(\frac{r_m^2}{R_o} \right) + P_o + \frac{1}{2} \left(\frac{r_m^2}{P_o} \right) - (R_o + P_o) = \frac{m\lambda}{2}. \quad (3.8)$$

To collimate the laser beam, P_o approaches infinity and Equation 3.8 reduces to

$$r_m^2 = R_o m \lambda \quad (3.9)$$

where R_o is the focal length of the Fresnel lens. The area of each Fresnel zone is approximately equal, therefore the transmission efficiency is approximately equal to 50%.

When the collimated light leaves the Fresnel lens the divergence angle of the laser beam is equal to the diffraction angle [3]. The divergence angle, θ , is calculated by

$$\theta = \frac{\lambda}{\pi \omega_o} \quad (3.10)$$

where λ is the wavelength of the laser light and ω_o is the diameter of the aperture of the Fresnel lens. For a λ of 780 nm and ω_o of 200 μm , θ equals 1.24×10^{-3} radians or 0.071 degrees.

3.4 Thermal Actuators

Thermal actuators have been extensively modeled and designed [4, 5, 6]. With deflection testing [4] and force testing [5], optimized actuators have been designed. The optimized actuators provide nearly ten microns of deflection. Further testing and development of thermal actuators have led to the design of the double arm thermal actuator [6]. The schematic for both the single hot arm and double hot arm actuator is shown in Figure 3-4. This design change allows the current to enter one hot arm and return on the second hot arm, eliminating the use of the cold arm and flexure to

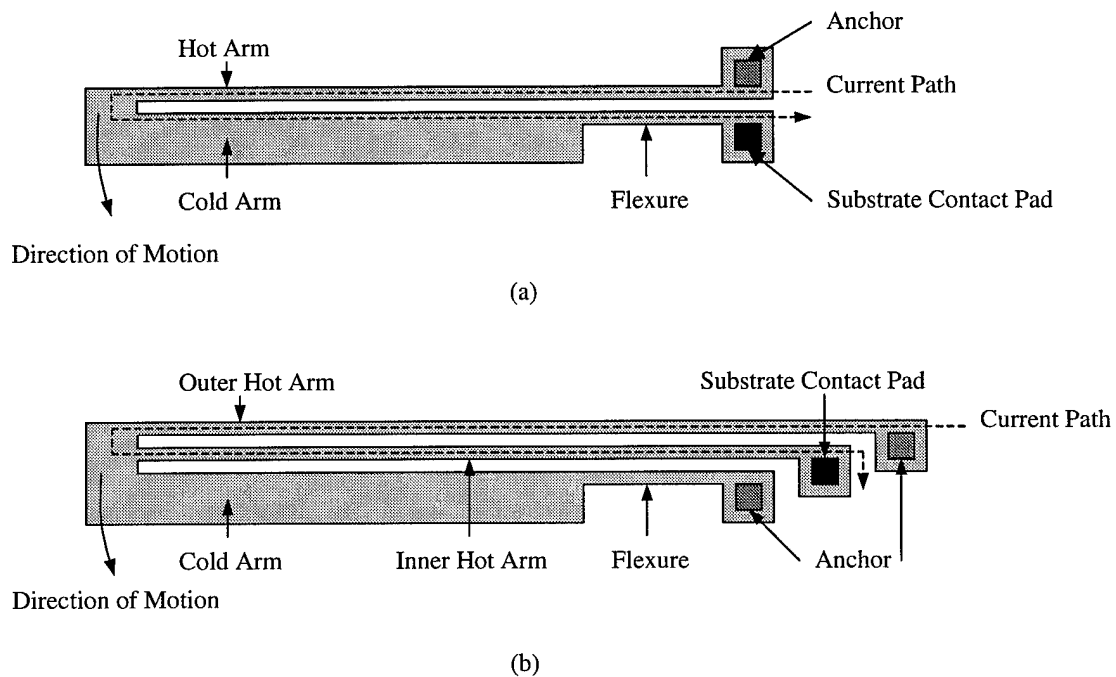


Figure 3-4. Schematic diagram of (a) single hot arm actuator, (b) double hot arm actuator [6].

complete the circuit. The outer arm of the double arm actuator is longer than the inner arm because the outer arm must expand more than the inner arm as the actuator rotates around the anchor of the cold arm. The double arm actuator is able to provide four

microns of deflection more than the single arm actuator [6]. Both designs are incorporated into the thermal arrays of the fan and rotating mirrors.

3.5 Mirrors

There are three mirrors used in the design of the scanner: fan mirror, rotating mirror, and 135° mirror. The fan mirror [5] and the rotating mirror [7] designs are locked into a position relative to the substrate and motion is provided by an array of thermal actuators. Figure 3-5 shows the triangle formed between the mirror, actuator array tether, and the substrate.

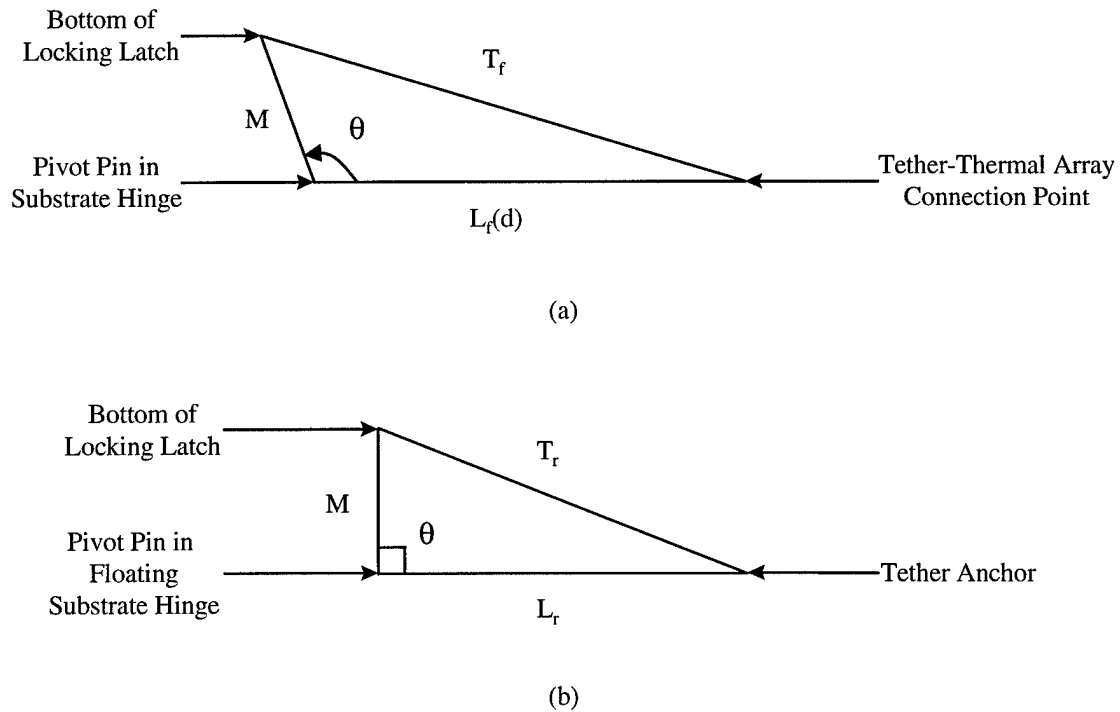


Figure 3-5. Triangle formed in design of (a) fan mirror and (b) rotating mirror.

In the case of the fan mirror, the angle between the mirror and substrate can be approximated by using the law of cosines. Using the triangle in Figure 3-5 (a), θ is calculated as

$$\theta = \cos^{-1} \left(\frac{M^2 - T_f^2 + L_f^2(d)}{2ML_f(d)} \right), \quad (3.11)$$

where M is the distance from the bottom of the pivot pin in the substrate hinge to the bottom of the tether lock, T_f is the length of the tether from the face of the mirror to the connection point of the thermal actuator array and $L_f(d)$ is the distance from the base of the mirror to the connection point of the thermal actuator array. $L_f(d)$ is a function of the deflection of the thermal actuator array, because the distance between the base of the mirror and the connection point changes when the thermal actuator array is actuated.

In the case of the rotating mirror, the angle between the mirror and the substrate must be 90° . The lengths of the sides of the triangle in Figure 3-5 (b) are given by the Pythagorean relation

$$T_r^2 = M^2 + L_r^2, \quad (3.12)$$

where M is the distance from the bottom of the pivot pin in the floating substrate hinge to the bottom of the tether lock, T_r is the length of the tether from the face of the mirror to the tether anchor and L_r is the distance from the base of the mirror to the tether anchor.

The 135° mirror is designed to fold over the VCSEL and form a 45° angle between the face of the mirror and the VCSEL. The design incorporates a two-part structure that forms the triangle shown in Figure 3-6. The distance, L , between the support and mirror along the substrate can be approximated by using the law of cosines. L is formulated as

$$L^2 + M^2 - 2LM \cos\theta = S^2, \quad (3.13)$$

where M is the distance from the bottom of the pivot pin in the substrate hinge to the

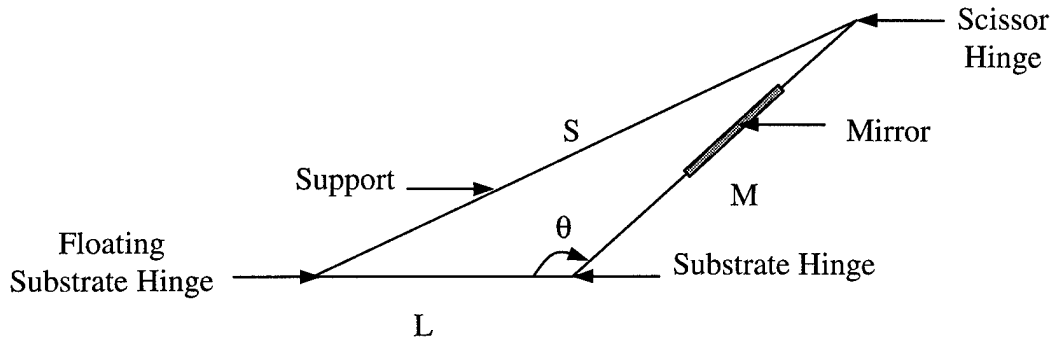


Figure 3-6. Triangle formed in design of 135° mirror.

beginning of the scissor hinge, S is the distance from the bottom of the pivot pin in the floating substrate hinge to the beginning of the scissor hinge and θ is equal to 135°. By rearranging Equation 3.13, L can be solved using the quadratic equation,

$$L^2 - (2M \cos\theta)L + (M^2 - S^2) = 0 \quad (3.14)$$

or

$$L = \frac{-b \pm \sqrt{b^2 - 4ac}}{2a}, \quad (3.15)$$

where $a = 1$, $b = (2M \cos\theta)$ and $c = (M^2 - S^2)$. Since the value of L can not be negative, only the positive value of L is used.

3.6 Range of Motion

The range of motion from the scanner in the X and Y directions can be determined by the far field pattern. The range of motion in both the lateral and vertical directions is shown in Figure 3-7. Using plane trigonometry for a right triangle the lateral scanning angle, θ , is calculated as

$$\tan \frac{\theta}{2} = \frac{X}{L} \quad (3.16)$$

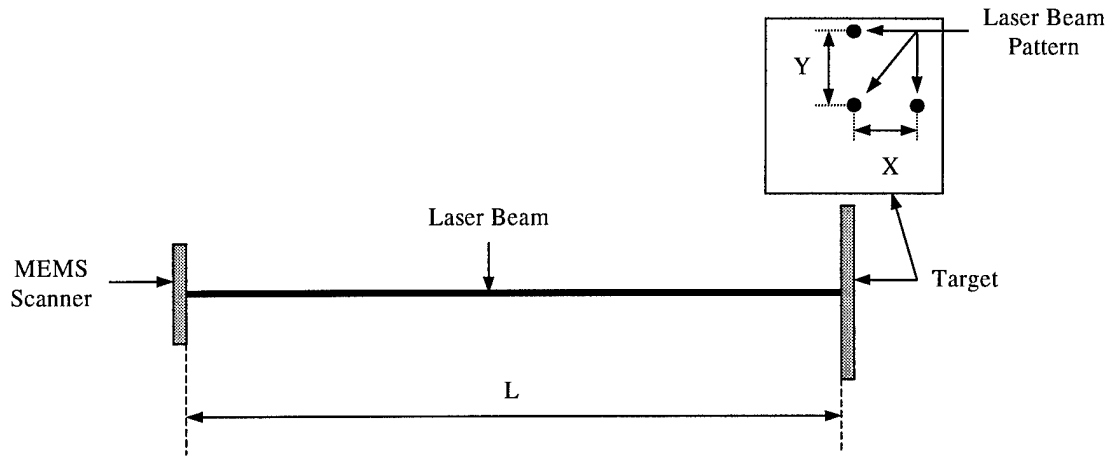


Figure 3-7. Range of motion of the scanner.

or

$$\theta = 2 \left(\tan^{-1} \frac{X}{L} \right). \quad (3.17)$$

Similarly the vertical scanning angle, ϕ , is calculated as

$$\phi = 2 \left(\tan^{-1} \frac{Y}{L} \right). \quad (3.18)$$

3.7 References

- [1] D. E. Sene, "Design, fabrication and characterization of micro opto-electro-mechanical systems" *Master's Thesis*, Air Force Institute of Technology, Wright-Patterson AFB, Ohio, AFIT/GEO/ENG/95D-03, December 1995.
- [2] K. D. Möller, *Optics*, University Science Books, California, 1988.
- [3] R. Guenther, *Modern Optics*, Wiley, New York, 1990.
- [4] J. H. Comtois, V. M. Bright and M. Phipps, "Thermal microactuators for surface-micromachining processes," *Proc. SPIE*, vol. 2642, pp. 10-21, October 1995.
- [5] J. R. Reid Jr., "Microelectromechanical isolation of acoustic wave resonators," *Doctoral Dissertation*, Air Force Institute of Technology, Wright-Patterson AFB, Ohio, AFIT/DS/ENG/96-12, December 1996.
- [6] D. M. Burns and V. M. Bright, "Design and performance of a double hot arm polysilicon thermal actuator," *Proc. SPIE*, vol. 3224, pp. 296-306, September 29-30, 1997.
- [7] J. R. Reid , V. M. Bright and J. H. Comtois, " A surface micromachined rotating micro-mirror normal to the substrate," *IEEE LEOS Summer Topical Meeting*, pp. 39-40, August 7-9, 1996.

Chapter 4

Experimental Setups, Procedures, and Design Descriptions

4.1 Introduction

This chapter covers the design process, design considerations, post-processing of the MEMS die, test equipment, testing procedures, and device and system descriptions. This chapter includes discussions of the designs fabricated, the devices' intended operational characteristics, and how each device was tested.

4.2 Design Process

The design process begins with design layout using a Computer Aided Design (CAD) tool. The CAD tool used at AFIT is the CADENCE layout editor in the Very Large Scale Integration (VLSI) Laboratory located in Building 640. The CADENCE layout editor has been customized with a MUMPs technology file, which defines the different MUMPs masking layers. The masking layers include POLY0, ANCHOR1, DIMPLE, POLY1, ANCHOR2, POLY1_POLY2_VIA, POLY2 and GOLD, which are represented by a different color in CADENCE. Drawing polygons in the different masking layers forms the designs. Figure 4-1 shows a typical CADENCE layout editor screen as seen on the computer monitor. The layout tool does not provide any checks for design rule errors. Checking for design errors is done both by the designer and by the AFIT MEMS group in a design review session. After the designs are completed and saved to a file, the file format is changed to the Caltech Intermediate Form (CIF), which is the format acceptable to MCNC. The file is sent to MCNC by electronic mail or by file transfer protocol.

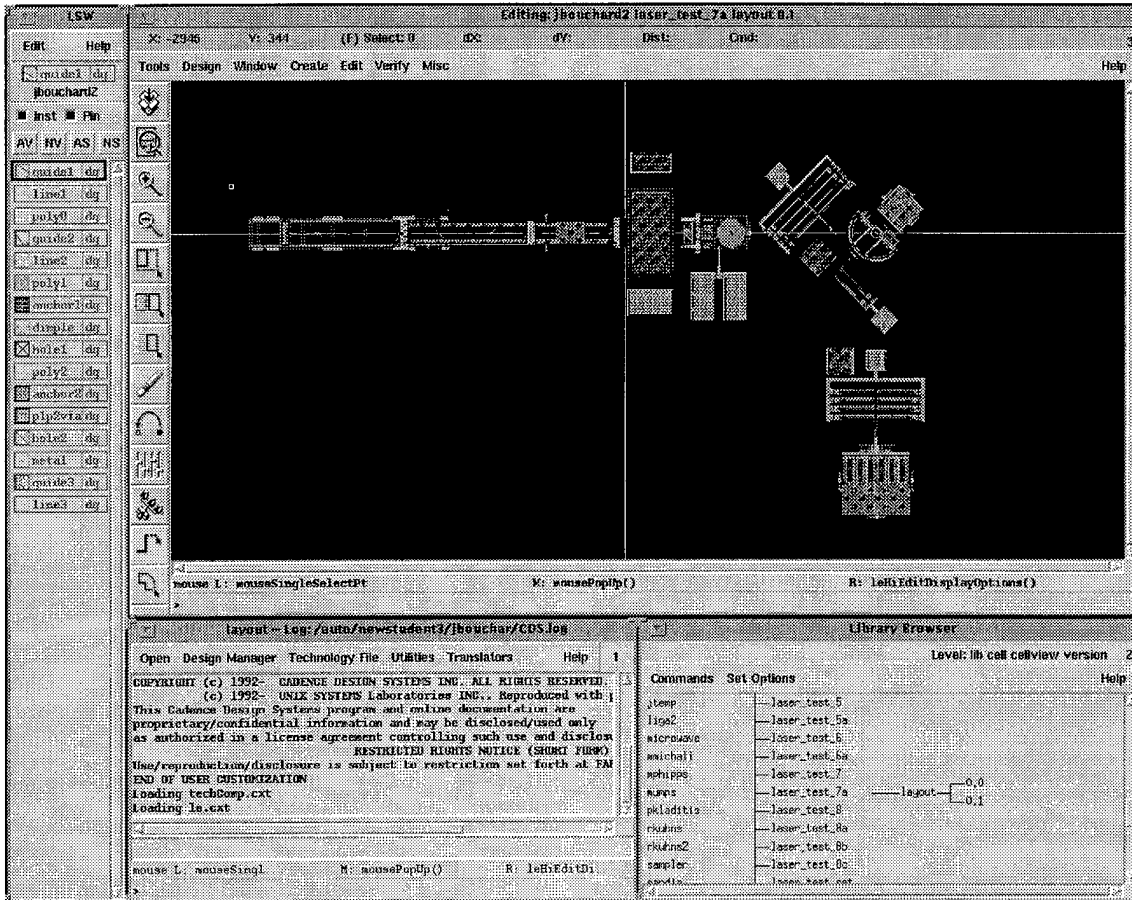


Figure 4-1. CADENCE layout editor screen of a MEMS scanner system.

The fabrication process at MCNC takes approximately two months. Before shipping the unreleased devices, the fabricated wafer is coated with a thick protective layer of photoresist and diced. MCNC produces about fifteen dice for each CIF file submitted. When the dice arrive some post processing is required to release the MEMS devices. The release procedure, shown in Table 4-1, removes the protective photoresist layer and then etches the sacrificial oxide layers. This release procedure allows the MEMS die to remain as clean as possible and reduces the possibility of devices being stuck to the substrate by capillary forces.

Table 4-1. Release Procedure for MUMPs Fabricated Die.

Step	Solution	Time	Remarks
1	Acetone #1	2 min.	Removes most of photoresist
2	Acetone #2	5 min.	Removes remaining photoresist
3	Methyl Alcohol #1	5 min.	Displace acetone from die
4	Hot Plate (90° C)	3 min.	Remove Methyl Alcohol
5	Hydrofluoric Acid (49% by wt.)	3-5 min.	Etches oxide
6	Deionized Water	3 sec.	Remove HF and stop etching
7	Methyl Alcohol #2	10-20 min.	Displace water from die
8	Hot Plate (90° C)	5 min.	Remove Methyl Alcohol

HydroFluoric (HF) acid, which is a hazardous chemical, is used in the release procedure. When HF acid comes in contact with the skin, it soaks through and attacks the calcium in the bones for which the only cure is removal of the effected area. Use of HF acid requires following certain precautions. The wear of rubber gloves, rubber apron, and eye protection is mandatory. All work with HF acid must be under the protection of a chemical vapor hood. Figure 4-2 shows the chemical vapor hood area where the release procedure is conducted.

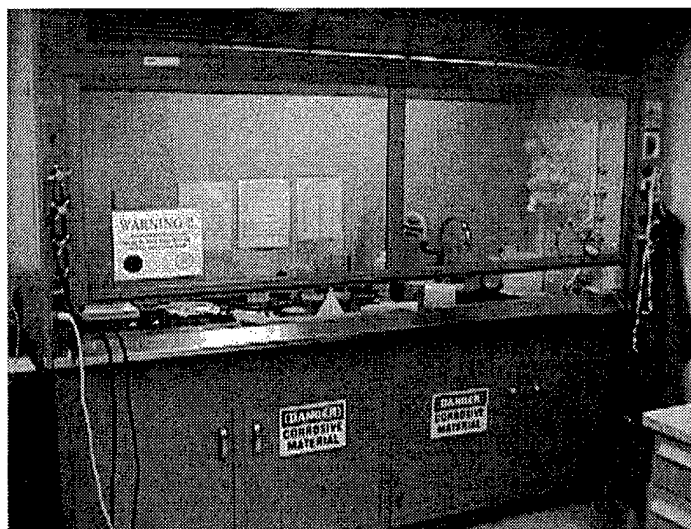


Figure 4-2. Chemical processing area used to release MEMS devices.

4.3 Design Considerations

There are several design considerations that must be taken into account due to the MUMPs fabrication method. The fabrication limitations are set forth by MCNC in their design guidelines and rules [1]. MCNC's lithography is based on masks, which are printed with a minimum dimension size of $0.25\ \mu\text{m}$. The minimum feature size of the polysilicon layers that can be designed in MUMPs is $2\ \mu\text{m}$. Together these rules pose no problem in the design of the larger structures, but the accuracy of Fresnel lens' focal length is limited due to the rounding of the calculations involved in determining the open and blocking zones of the Fresnel zone plate.

Another design consideration is the large structures require etch holes. Etch holes provide more access to the sacrificial layers so that all of the oxide is removed from under the structure during the etching to ensure a complete release. The design guidelines recommend etch holes be placed every $30\ \mu\text{m}$, although devices designed with $100\ \mu\text{m}$ spacing have been successfully released.

The effect of surface topology on thin film layers is another design consideration. The topology shown in Figure 4-3 is the result of patterning a polysilicon layer with each

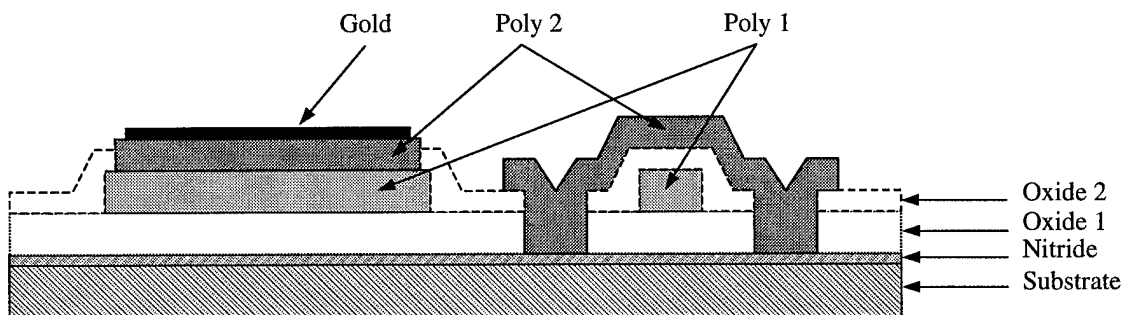


Figure 4-3. A cut away view of a flip-up mirror with a substrate hinge.

successive layer conforming to the previous layer. In this example the Poly 2 layer conforms around the Oxide 1, Oxide 2 and Poly 1 layers, constraining the Poly 1 pin inside the Poly 2 substrate hinge.

The final design consideration is physical positioning of devices, bond pads, and flip-up helpers. There are many tradeoffs to consider when placing designs on a die. Ultimately the devices should be packed densely enough to allow for as many designs as possible to be placed on the die, but not so dense that assembling the devices is hampered. The positioning of the devices must also allow for bond pads and wiring. The bond pads enable the die to be wire bonded to a chip carrier, which allows for ease of testing the devices. Finally, specially designed flip-up helpers enable the devices to be raised slightly in order to get a probe tip underneath the device in order to assemble it.

4.4 Testing Equipment

The following list of test equipment was used during post-processing, assembling, testing, and characterization of the devices on the MEMS die.

Micromanipulator Table – The Micromanipulator Company, Model 6200

The micromanipulator allows for assembling and testing of the MEMS devices on a released die. The micromanipulator station consists of an air table, microscope, vacuum pump, up to eight probes, and a video camera. Figure 4-4 shows the micromanipulator station. The station floats on an air table to isolate the microscope and probes from vibrations in the surrounding area. The Device Under Test (DUT) is placed on the circular stage of the microscope. The microscope has four objective lenses (2.25X, 8X, 25X, 50X) for viewing the DUT. The stage allows two-dimensional motion parallel to

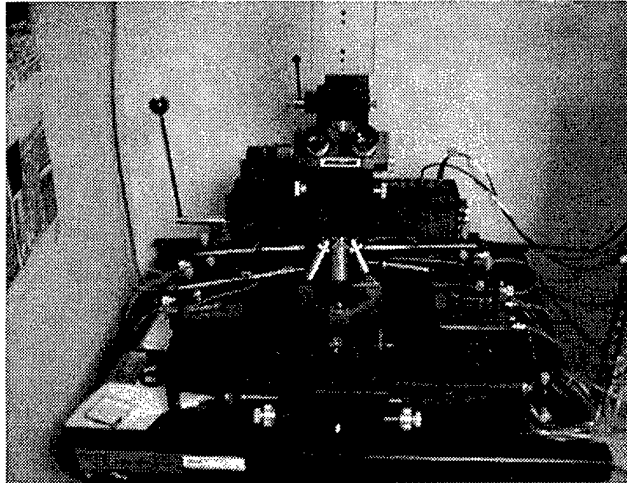


Figure 4-4. Micromanipulator station, Model 6200.

the surface plane of the die as well as allowing the die to rotate around the center of the stage. The microscope can move in three dimensions while the stage is held in place. The surface on which the probes sit is adjustable perpendicular to the face of the die. A vacuum is provided by a pump to the stage in order to hold the die securely in place and to each of the probe bases to hold them securely in place and reduce unnecessary vibrations while moving the probe tips. The probes used have a tip diameter of 5 μm and are utilized during the assembling and testing of the devices. The probe tips also supply the electrical connection to a customized test panel, which can interface with voltage sources and test equipment. Video can be taken of the DUT through a camera mounted on top of the microscope.

Micromanipulator Table with a Class I Laser Cutter - The Micromanipulator Company, Model LAS-2001

This micromanipulator station provides the same things as the Model 6200 except it contains a Class I Laser Cutter, allows up to six probes, and four objective lenses (2X,

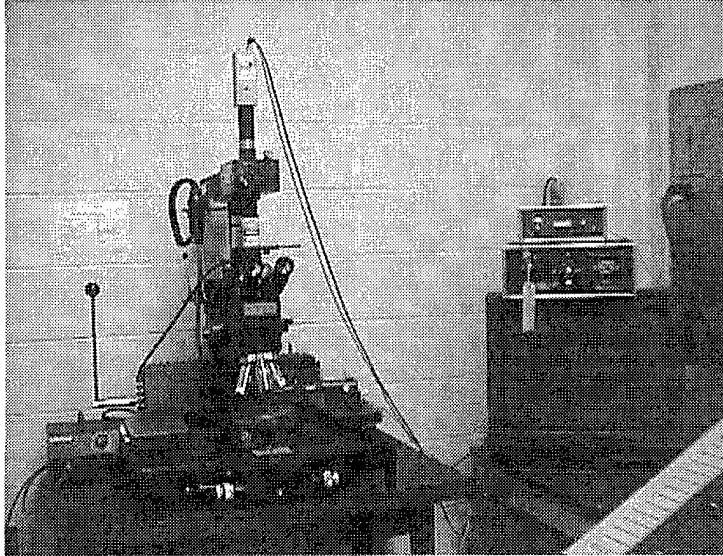


Figure 4-5. Micromanipulator station, Model LAS-2001.

10X, 20X, 80X). Figure 4-5 shows the micromanipulator station. The laser provides a visible green beam (532 nm) which can be adjusted from 1 to 16 microns in diameter. The energy output of the laser, depending on the diameter of the beam is between 10^{-8} - 10^{-4} J. The laser can provide a single or a continuous stream of pulses. The pulse duration lasts 8 ns and the minimum time between successive pulses is 1s. The laser allows removal of unwanted material by vaporizing without melting, which can be used to cut additional etch holes in a large device or correct other design flaws.

Scanning Electron Microscope - International Scientific Instruments, Model WB-6

The Scanning Electron Microscope (SEM) is used to obtain three-dimensional pictures of MEMS devices. Figure 4-6 shows the SEM. The SEM has a resolution capability of approximately 4 nm. The SEM consists of a vacuum chamber, vacuum pumps, water cooling system, control panel, and Polaroid camera. To improve the image quality and reduce charge buildup, a thin film of gold must be sputtered on MEMS die before using

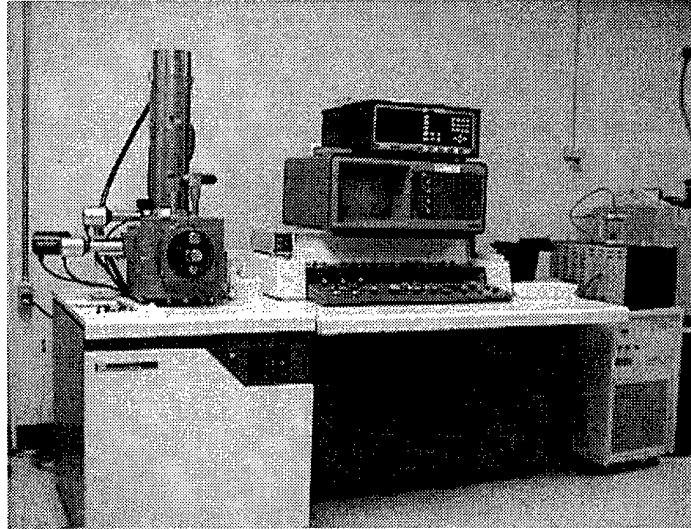


Figure 4-6. Scanning electron microscope, Model WB-6.

the SEM. The die is placed on a holder in the vacuum chamber. The holder can be moved in three dimensions as well as being able to be tilted and rotated. The pictures taken are on a 4X5 inch sheet film.

Sputterer - Ladd Research Industries, Inc., Model 30800

The bench top sputterer, shown in Figure 4-7, is used to deposit a thin film of gold on

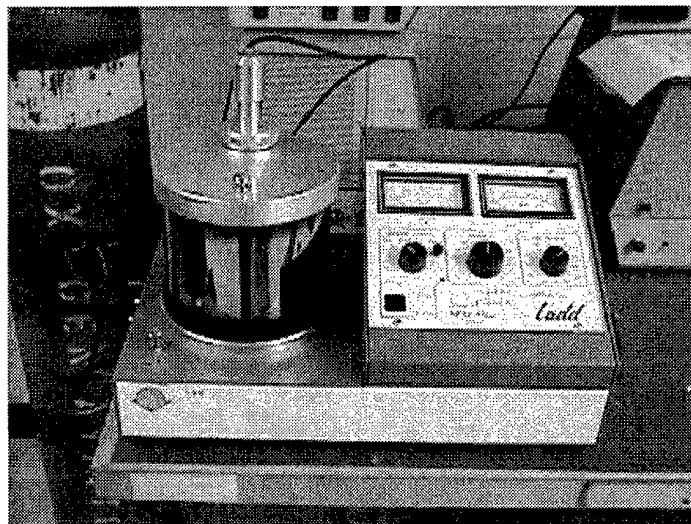


Figure 4-7. Bench top sputterer, Model 30800.

a MEMS die. The sputterer consists of a vacuum chamber, vacuum pump, gold target, and a tank of argon gas. The thickness of the gold applied to the MEMS die is approximately 200 Å. This is accomplished by obtaining a vacuum of 0.1 Torr in the chamber and applying 2.2 KV at 20 mA to the gold target for 2 minutes. The current, 20 mA, is maintained by adjusting the flow of argon into the chamber.

Ball Bonder - Kulicke and Soffa Industries, Inc., Model 4124

The ball bonder, shown in Figure 4-8, was used to solder in the VCSEL, provide electrical contact from the VCSEL to the MEMS die, and provide electrical contacts from

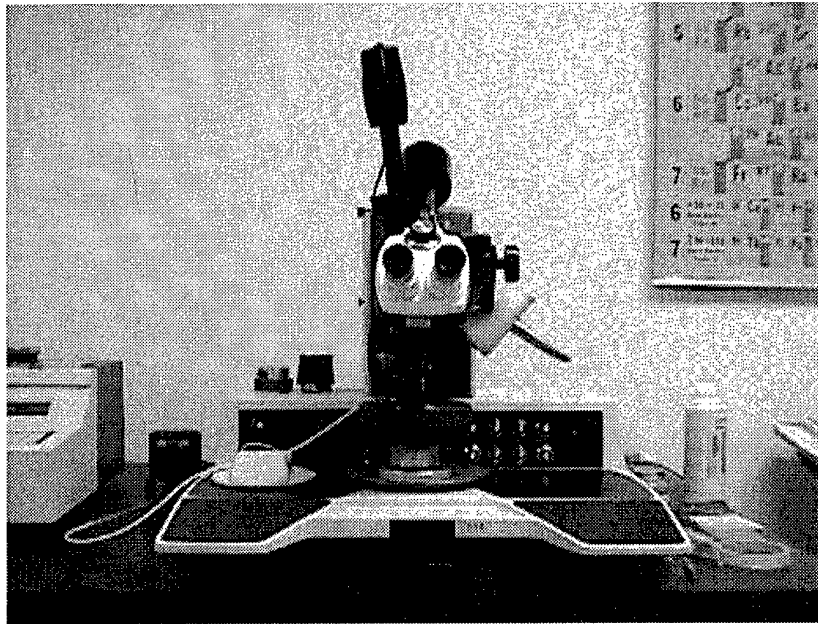


Figure 4-8. Ball Bonder, Model 4124.

the MEMS die to a chip carrier. Soldering the VCSEL to the MEMS die is discussed in Chapter 5. The bonder uses temperature, pressure, and high frequency vibration to bond a 25 µm gold wire. The first bond is ball bond, which is used on the bond pad of the MEMS die and the second is a wedge bond, which is used on the pads of the chip carrier.

Optical Power Meter - Coherent Fieldmaster, Model FM

The optical power meter is a digital device, which was used to measure the optical power of the VCSEL and the MEMS scanner system. Figure 4-9 shows the optical power meter and the optical detector. The optical power meter can measure optical power up to 20 mW.

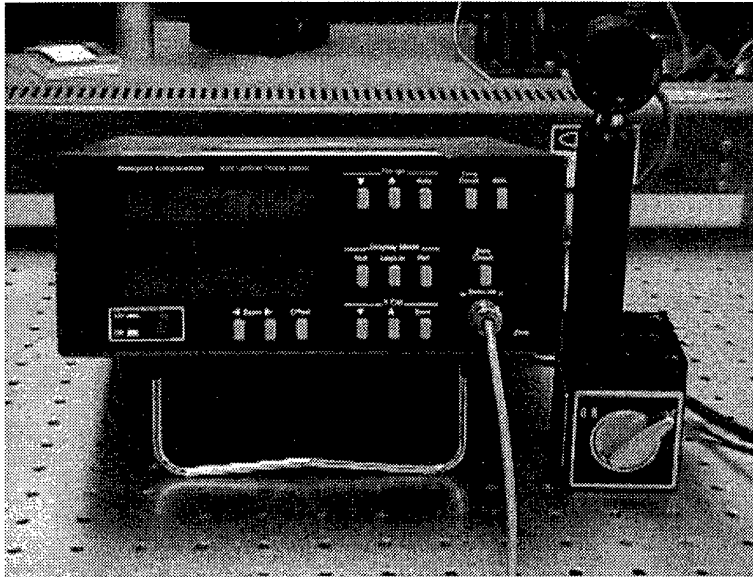


Figure 4-9. Optical power meter, Model FM.

Triple Output Power Supplies - Hewlett Packard, Model HP6236B

The power supply provides two independently adjustable voltages or current sources. The first supplies a positive 6 VDC, while the other provides a ± 20 VDC. The current is adjustable up to ± 2.5 A.

Multimeter – Fluke, Model 8600A

The multimeter is the primary test equipment for reading resistance, voltage, and current of DUT. The multimeter is capable of measuring voltage up to 750 VAC or 1000 VDC, current up to 10 A, and resistance up to 32 M Ω .

4.5 Test Setups

The assembling and testing of devices were completed on the micromanipulator station. The preliminary testing of the MEMS system can also be completed on the micromanipulator station. Testing the MEMS system for its range of motion requires the die to be mounted and wire bonded to a 144 pin chip carrier, shown in Figure 4-10. A

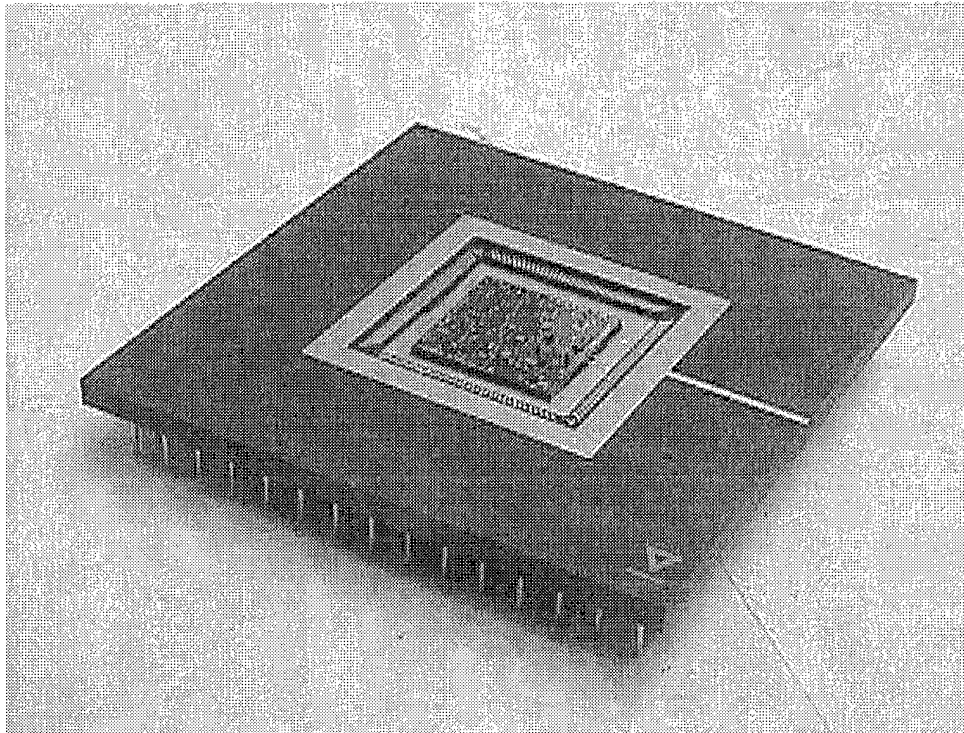
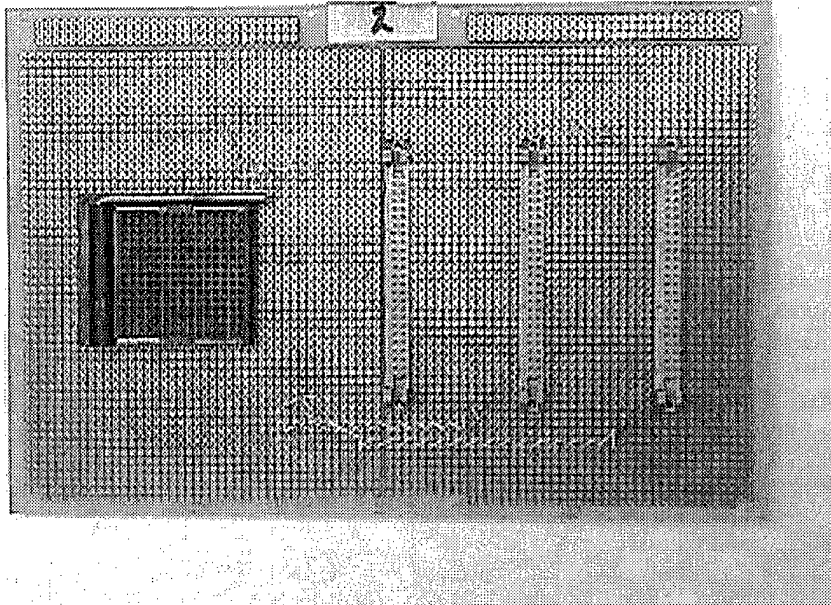
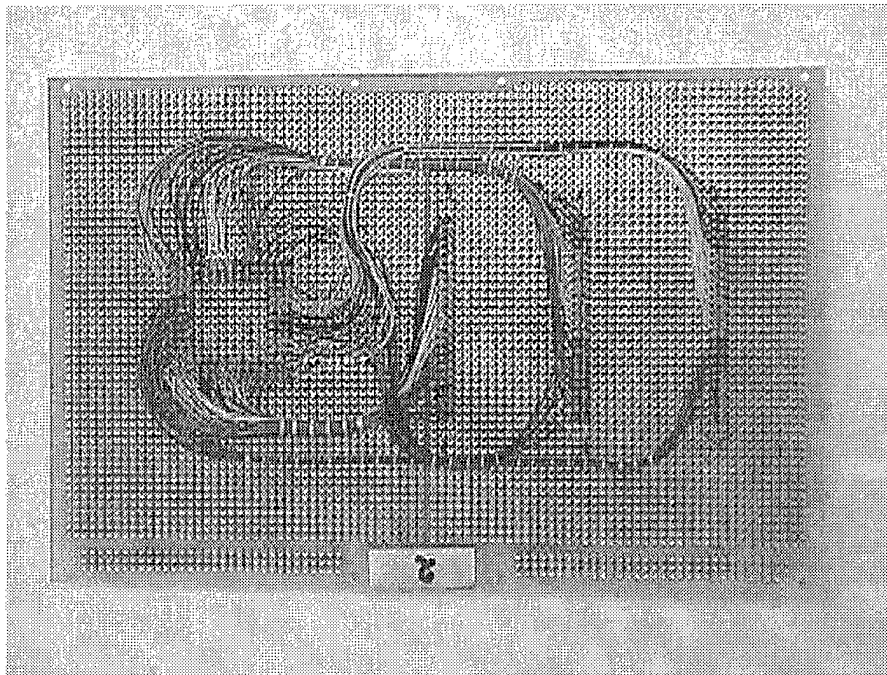


Figure 4-10. 144 pin chip carrier with a MEMS die mounted and wire bonded.

test structure for holding the chip carrier was also required. The test structure, shown in Figure 4-11, is made up of a solderless breadboard, a zero insertion force socket, and three 50 pin connectors. The electrical connections between the connectors and the socket are provided by strands of 30 gauge wire. The wires are wire wrapped to each connector and secured to the breadboard to prevent the wires from being pulled off their connectors.



FRONT



BACK

Figure 4-11. Test structure for testing the MEMS die mounted in a 144 pin chip carrier.

4.6 Device Descriptions

This section outlines in detail the major devices designed for this thesis. The designs were fabricated in MUMPs runs 18 through 20. A CADENCE layout of each design is provided with a SEM picture of the fabricated device.

4.6.1 VCSEL Pad

The VCSEL pad, see Figures 4-12 and 4-13, is used to help align the VCSEL when attaching it to the MEMS die and provide electrical contact for the VCSEL. The substrate pad is made by breaching the Nitride layer and is used to provide electrical contact with the bottom contact of the VCSEL. This is accomplished by using the Reactive Ion Etching (RIE) from the MUMPs. The RIE over-etches the masking layer to ensure that all the masking layer is removed. When ANCHOR1, ANCHOR2, DIMPLE, and POLY1_POLY2_VIA masks are placed over an area without Poly 0 or Poly 1, the result is a breach in the Nitride layer with approximately 3 μm of the substrate removed. The substrate pad then gets a Poly 2 and Gold layer. The dimensions of the hole, Poly 2, and Gold are 610X300 μm , 600X290 μm , and 590X280 μm , respectively. The alignment guide is made of stacked Poly 1 and Poly 2, and is 20 μm wide and its inside dimensions are 620X310 μm .

The wire bonding pad is a standard bonding pad which provides an area to make a wire bond to the top electrical contact of the VCSEL. The wire bonding pad is made of Poly 0, Poly 2, and Gold with the dimensions of 350X195 μm , 342X187 μm , and 336X181 μm , respectively. The low resistance wire provides electrical connection between this wire bonding pad and a wire bonding pad located at the edge of the MEMS die. The wire

is made of Poly 0 (24 μm wide), Poly 2 (20 μm wide), and Gold (17 μm wide).

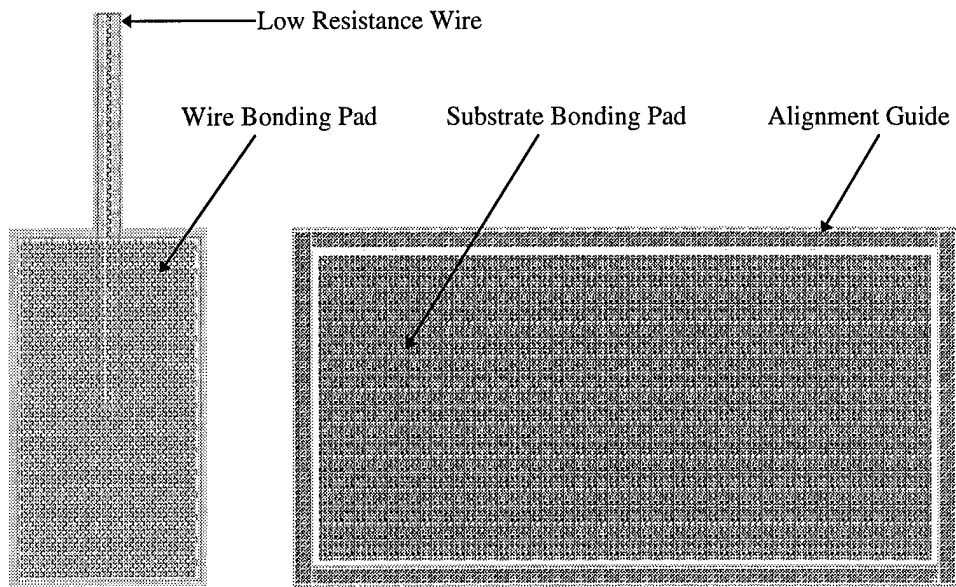


Figure 4-12. CADENCE layout of the VCSEL pad.

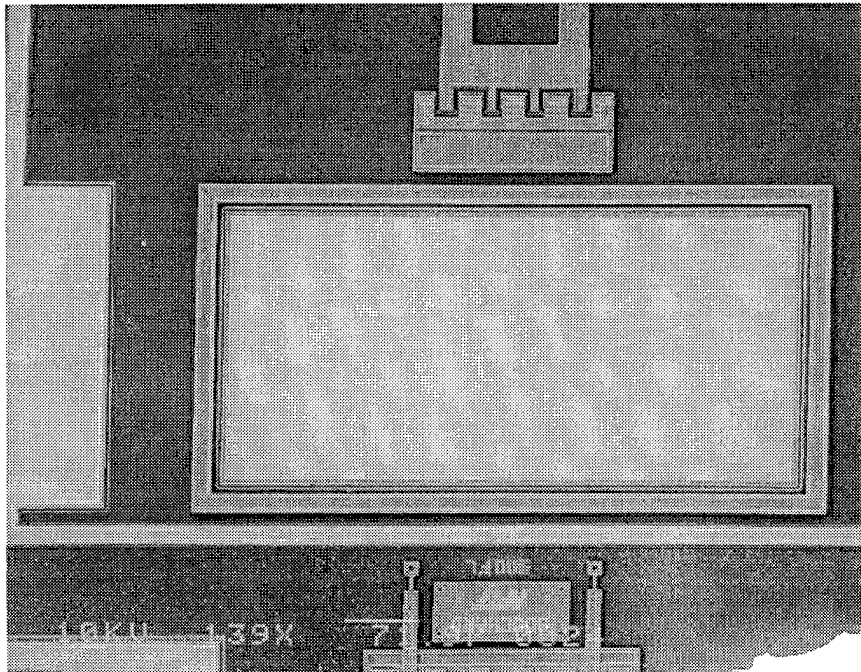


Figure 4-13. Scanning electron micrograph of VCSEL pad.

4.6.2 135° Mirror

The 135° mirror, see Figures 4-14 and 4-15, is designed to flip up over the VCSEL to redirect the laser beam 90°. The mirror consists of three major parts; guide rail (Poly 1 rail and Poly 2 rail guides), elevating arm (Poly 1, Poly 2 stack), and mirror arm (Poly 1, Poly 2 stack). The guide rail is used to assemble and lock the mirror in place. The guide

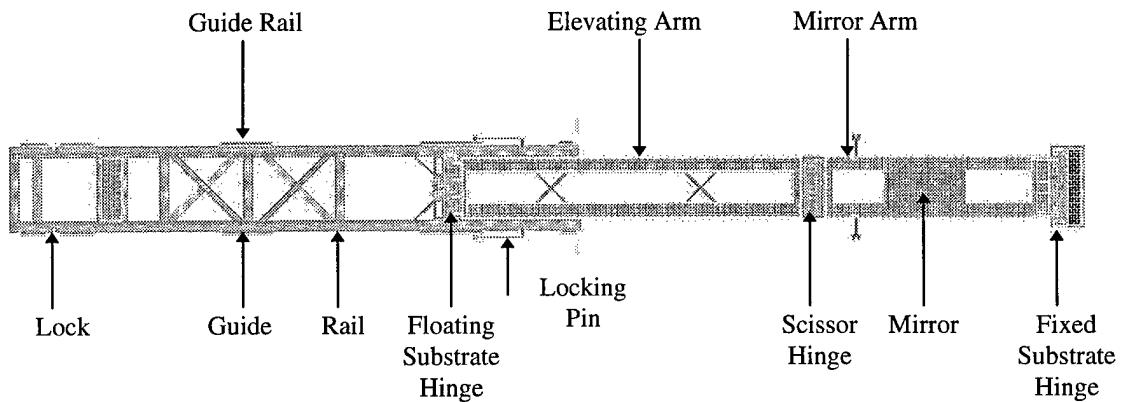


Figure 4-14. CADENCE layout of the 135° mirror.

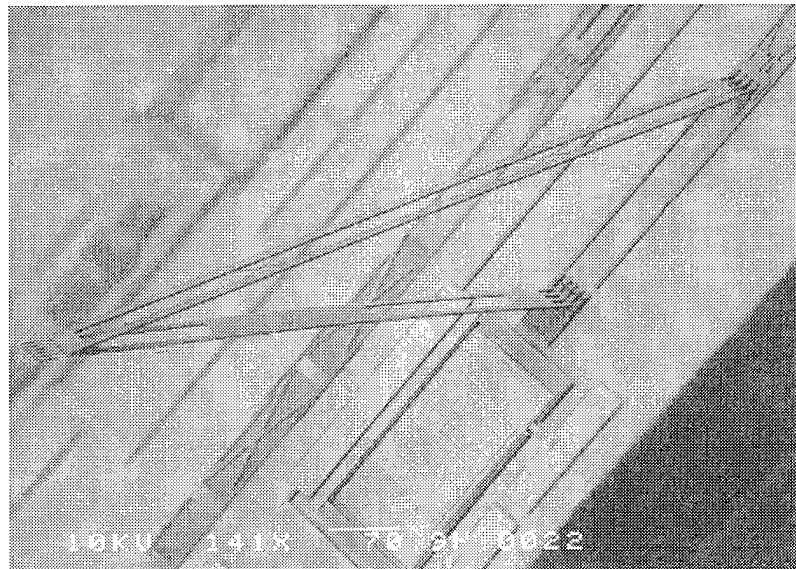


Figure 4-15. Scanning electron micrograph of assembled 135° mirror over a VCSEL bonding pad.

rail moves the base of the elevating arm to a position $375.5 \mu\text{m}$ from the base of the mirror arm, which satisfies Equation 3.14. The elevating arm, which is connected to the guide rail by a floating substrate hinge and the mirror arm by a scissor hinge, elevates the mirror arm off the substrate and over the VCSEL. The elevating arm is $924.5 \mu\text{m}$ from the base to the bottom of the scissor hinge. The mirror arm is attached to the substrate by a fixed substrate hinge and is $620 \mu\text{m}$ from the base to the bottom of the scissor hinge. The mirror on the mirror arm is $200 \times 151 \mu\text{m}$ and the center is located $353.5 \mu\text{m}$ from the base of the mirror arm. The mirror is located approximately $150 \mu\text{m}$ from the VCSEL aperture, so by Equation 3.3 the worst case ($D_1 = 10 \mu\text{m}$ and $\theta = 10^\circ$) diameter of the beam is $62.9 \mu\text{m}$. There are four etch holes ($4 \mu\text{m}$ squares) on the mirror and they are located $48 \mu\text{m}$ in from the sides and $67 \mu\text{m}$ in from the top and bottom.

4.6.3 Fresnel Lens

The Fresnel lens, see Figures 4-16, 4-17, and 4-18, is used to collimate the laser beam from the VCSEL. The Fresnel lens is designed out of Poly 2 and coated with gold. The design of the Fresnel lens is based on focal length of $500 \mu\text{m}$. Using Equation (3.10) the open and blocking zones were determined. The center of the Fresnel lens is $250 \mu\text{m}$ off the surface of the die, which is where the center of the laser beam comes off the 135° mirror. The lens is attached to the substrate by a substrate hinge. To ensure the Fresnel lens would be locked into position with an angle of 90° with respect to the substrate, the microlatch was designed using Equation 3.13. The bottom of the locking slot is $19 \mu\text{m}$ from the bottom of the hinge pivot pin. The latch is $111 \mu\text{m}$ from the latch anchor to notch in the latch and is anchored $109.5 \mu\text{m}$ from the base of the Fresnel lens. The design

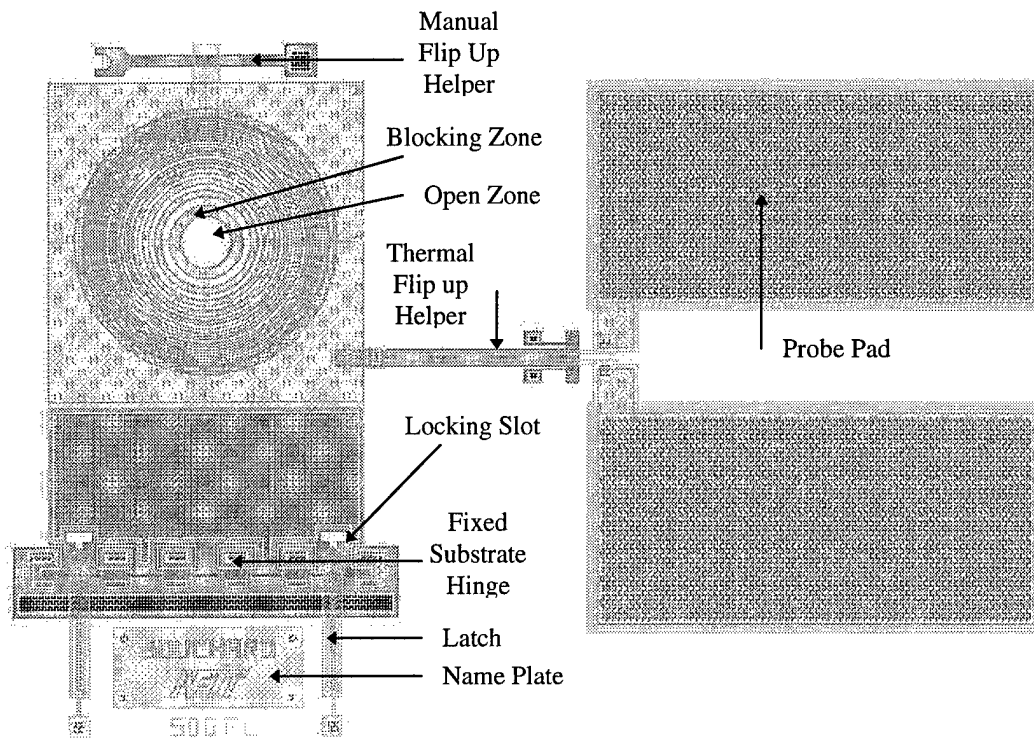


Figure 4-16. CADENCE layout of the Fresnel lens.

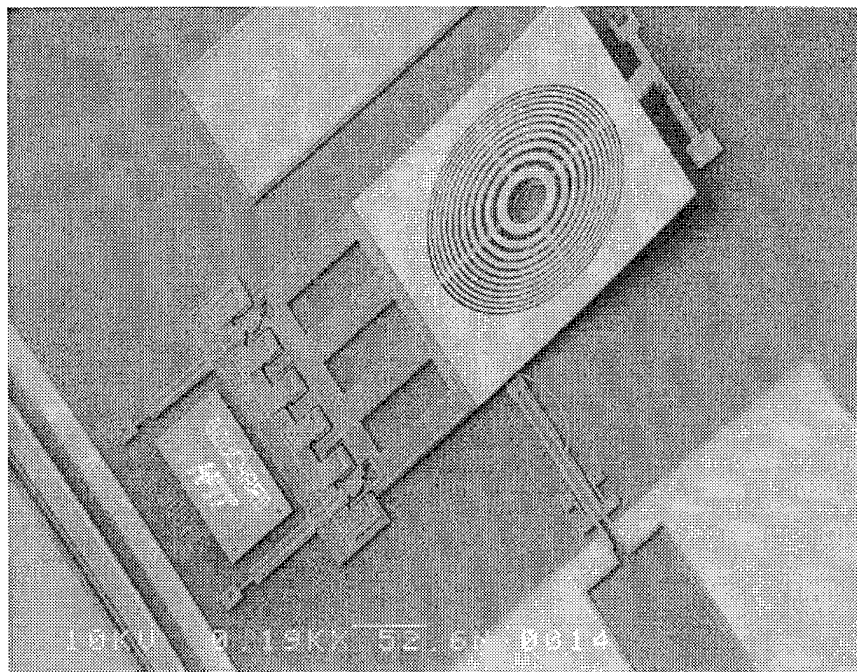


Figure 4-17. Scanning electron micrograph of Fresnel lens.

of the Fresnel lens also includes two different types of flip up helpers. There is a manual flip-up helper located on the top of the lens. The other flip-up helper is a thermal actuator, which when back bent lifts the lens up off the substrate. The Fresnel lens is a $240\ \mu\text{m}$ square plate with an aperture diameter of $189.5\ \mu\text{m}$. Using Equation 3.3 in the worst case ($D_1 = 10\ \mu\text{m}$ and $\theta = 10^\circ$), the diameter of the beam at the face of the Fresnel lens is $186.3\ \mu\text{m}$. Using Equation 3.11, the divergence angle out of the Fresnel lens is 0.071° .

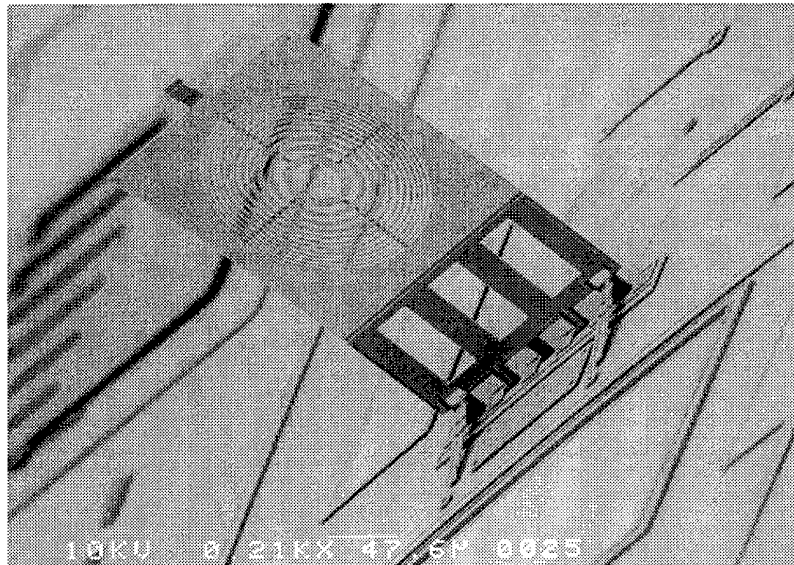


Figure 4-18. Scanning electron micrograph of assembled Fresnel lens.

4.6.4 Rotating Mirror

The rotating mirror, see Figures 4-19, 4-20, and 4-21, is used to scan the laser beam parallel to the substrate. The mirror is designed out of stack Poly 1 and Poly 2 coated with Gold. The mirror is $230 \times 230\ \mu\text{m}$ with the center of the mirror $250\ \mu\text{m}$ above the substrate. Using Equation 3.3, the diameter of the laser beam when it reaches the rotating mirror is between $191.5 - 193.0\ \mu\text{m}$, depending on which laser system is being

used. The mirror has sixteen $4\ \mu\text{m}$ square etch holes centered every $50\ \mu\text{m}$. The rotating mirror was designed with three manual flip-up helpers. The rest of the mirror support and

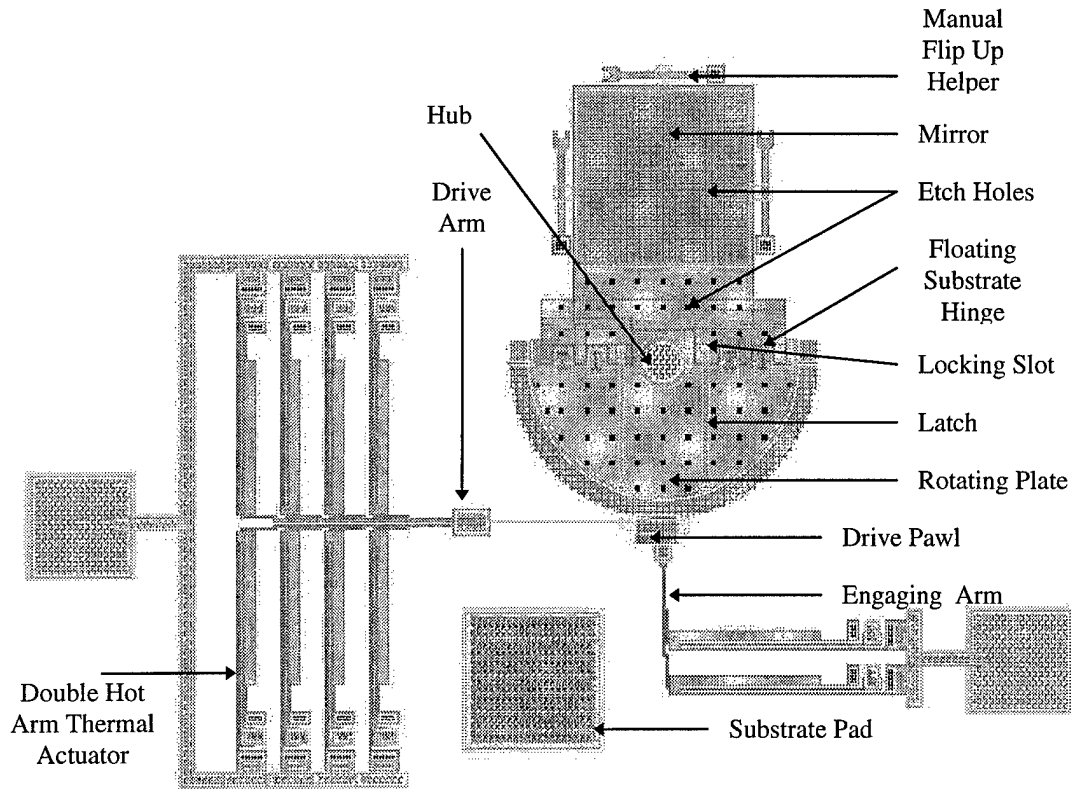


Figure 4-19. CADENCE layout of the rotating mirror.

the rotating plate is made out of Poly 1 with $5\ \mu\text{m}$ square etch holes centered every $35\ \mu\text{m}$. To ensure the rotating mirror will lock into position with an angle of 90° with respect to the substrate, the microlatch was designed using Equation 3.13. The bottom of the locking slot is $14.5\ \mu\text{m}$ from the bottom of the hinge pivot pin. The latch is $160.7\ \mu\text{m}$ from the latch anchor to notch in the latch and is anchored $160\ \mu\text{m}$ from the base of the rotating mirror. There are four different designs of the rotating mirrors, which combine either single or double hot arm thermal actuator arrays with the mirrors oriented at an offset angle of 0° or 45° with respect to the path of the laser beam.

The operation of the rotating mirror, see Figure 4-22, requires two overlapping signals applied to the thermal actuators of the drive pawl and the engaging arm. The rotating plate rotates when power is applied to the thermal actuators of the drive pawl and the

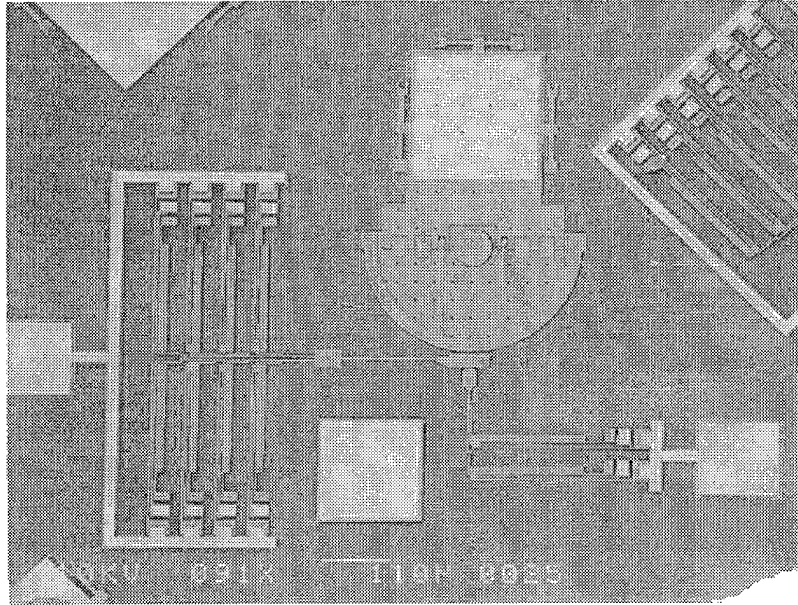


Figure 4-20. Scanning electron micrograph of rotating mirror.

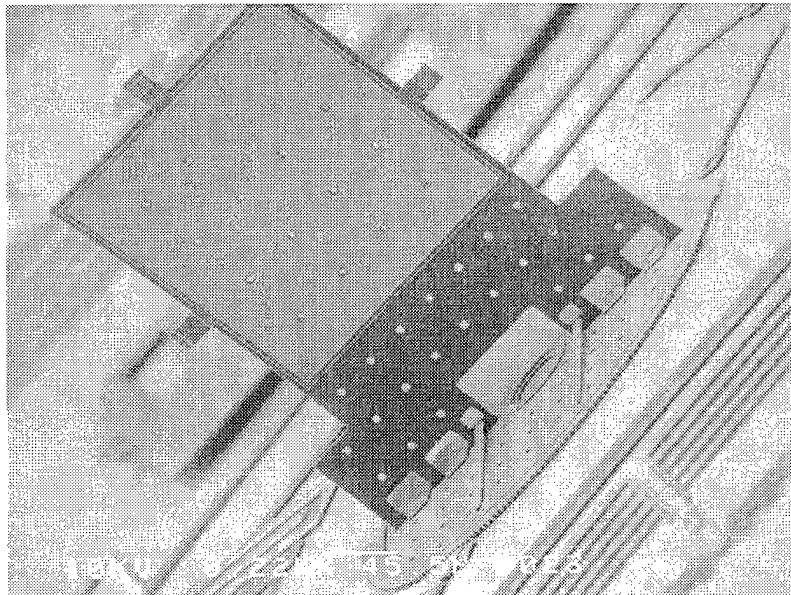


Figure 4-21. Scanning electron micrograph of assembled rotating mirror.

thermal actuators of the engaging arm. When power is applied to the thermal actuators, either the drive pawl or the engaging arm is extended. The drive pawl is extended before the engaging arm moves the drive pawl into contact with the rotating plate. Once the drive pawl is in contact with the rotating plate the power is removed from the drive arm and the rotating plate is pulled by the drive pawl in a clockwise direction. The power is then removed from the engaging arm. This is repeated to continue the clockwise rotation. Counter clockwise rotation is accomplished by applying power to the engaging arm before applying power to the drive pawl.

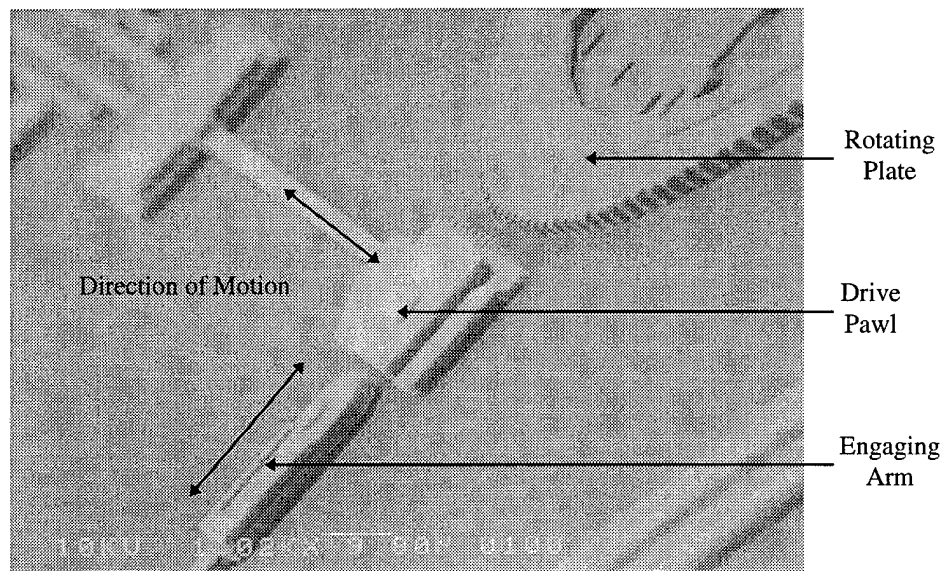


Figure 4-22. Scanning electron micrograph of rotating mirror's drive mechanism.

4.6.5 Fan Mirror

The fan mirror, see Figures 4-23, 4-24, and 4-25, is used to scan the laser beam perpendicular to the substrate. The fan mirror is designed out of stacked Poly 1 and Poly 2 coated with Gold. The mirror is 230X497 μm with the center of the mirror 250 μm above the substrate, when mirror is positioned at an angle of 135° with respect to the

substrate. Using Equation 3.3, the diameter of the laser beam when it reaches the rotating mirror is approximately 195 - 197.5 μm , depending on which laser system is

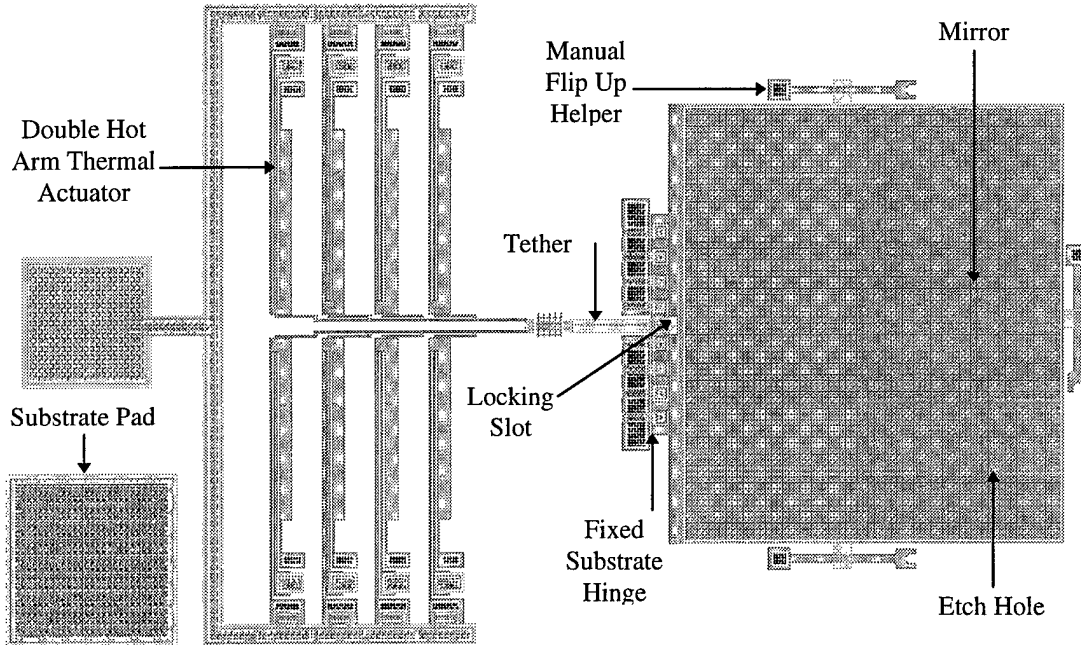


Figure 4-23. CADENCE layout of the fan mirror.

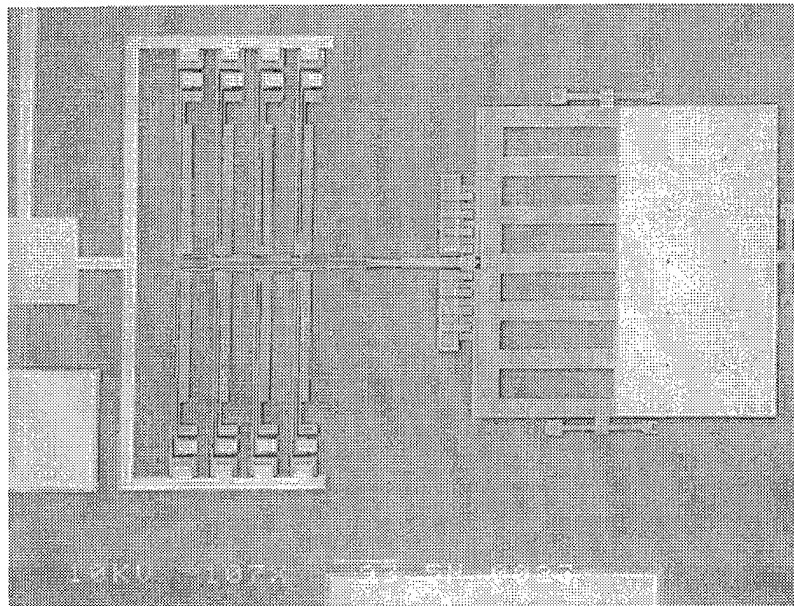


Figure 4-24. Scanning electron micrograph of fan mirror.

being used. The mirror has ten $4\ \mu\text{m}$ square etch holes centered approximately every $83\ \mu\text{m}$. The fan mirror was designed to be locked into position with an angle of 125° with respect to the substrate so the microlatch was designed using Equation 3.12. The

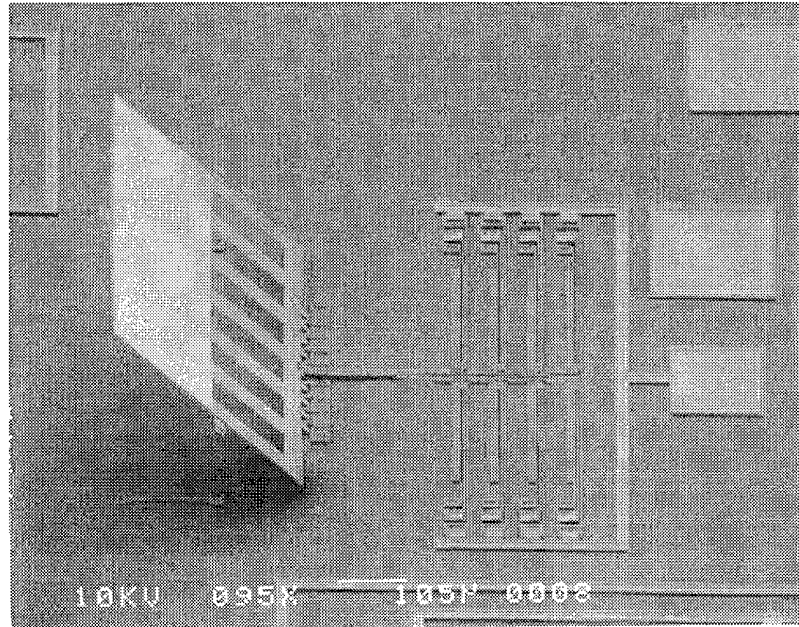


Figure 4-25. Scanning electron micrograph of assembled fan mirror.

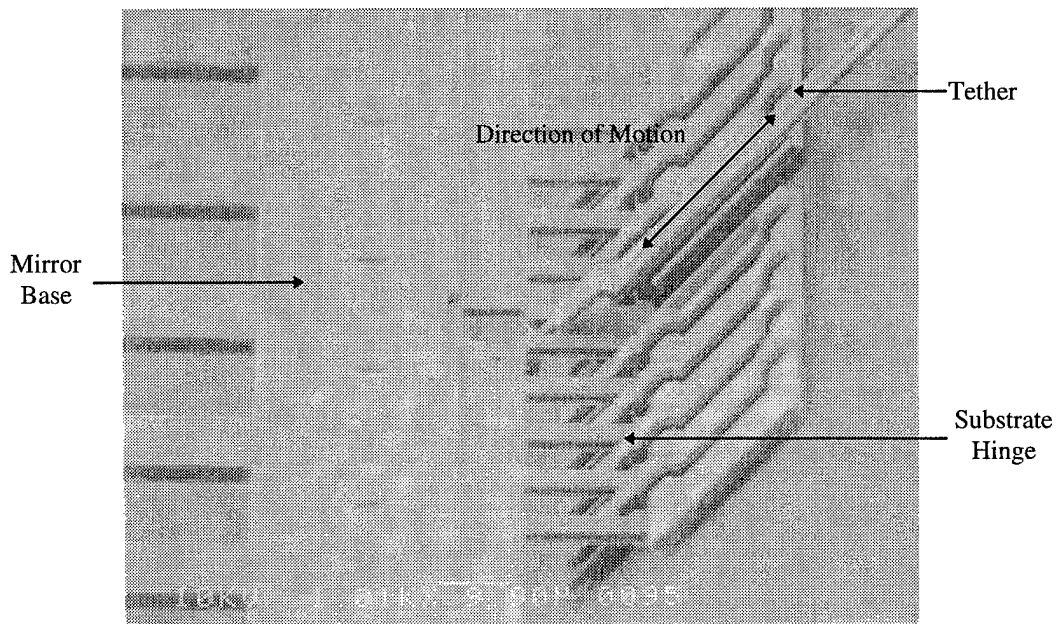


Figure 4-26. Scanning electron micrograph of fan mirror's drive mechanism.

bottom of the locking slot is 15 μm from the bottom of the hinge pivot pin. The tether is connected to the thermal actuator array 145 μm from the base of the fan mirror so distance from the face of the mirror to the connection point of the thermal array is 154 μm . There are two different designs of the fan mirrors, which combine either single or double hot arm thermal actuator arrays with the mirrors. The operation of the fan mirror, see Figure 4-26, is much simpler than the rotating mirror. Applying power to the thermal actuators allows the tether to be extended, increasing the angle between the fan mirror and the substrate. When the power is removed the tether retracts and the fan mirror returns to its original position.

4.7 References

1. D. A. Koester, R. Mahadevan, A. Shishkoff and K. W. Markus, " SmartMUMPs Design Handbook including MUMPs Introduction and Design Rules (rev. 4)," MCNC Internet website, <http://mems.mcnc.org/smumps/SMTOC.html>, MEMS Technology Application Center, MCNC, NC, July 1996.